NUCLEAR SCIENCE AND ENGINEERING: **146**, 13–50 (2004)

Impact of Nuclear Data Uncertainties on Transmutation of Actinides in Accelerator-Driven Assemblies

G. Aliberti, G. Palmiotti, M. Salvatores,*† and C. G. Stenberg

Argonne National Laboratory
Nuclear Engineering Division, Building 208
9700 South Cass Avenue
Argonne, Illinois 60439

Received October 15, 2002
Accepted May 8, 2003

Abstract—*The potential impact of nuclear data uncertainties on a large number of performance parameters of reactor cores dedicated to the transmutation of radioactive wastes is discussed. An uncertainty analysis has been performed based on sensitivity theory, which underlines the cross sections, the energy range, and the isotopes that are responsible for the most significant uncertainties.*

To provide guidelines on priorities for new evaluations or validation experiments, required accuracies on specific nuclear data have been derived, accounting for target accuracies on major design parameters. The required accuracies (mostly in the energy region below 20 MeV), in particular for minor actinide data, are of the same order of magnitude of the achieved accuracies on major actinides. Specific requirements also concern the improvement of minor actinide data related to decay heat and effective delayed-neutron fraction assessment.

I. INTRODUCTION

Among the strategies for radioactive waste management, the so-called partitioning and transmutation (P/T) strategy has attracted considerable interest in the last decade, and relevant studies have been performed in several leading laboratories, sometimes under the coordination of international organizations (see, for example, Ref. 1). Most of the studies have pointed out the role of minor actinide (MA) transmutation to reduce the source of potential radiotoxicity in deep geological storage and of long-lived fission product transmutation in order to eventually reduce the so-called residual risk.[1] In both cases, the transmutation should be performed in a neutron field, preferably with a fast neutron spectrum.[2] Among the different scenarios of implementation of the P/T strategy, there has been a remarkable convergence on two major options,[3,4] namely, the use of standard critical fast reactors, where, for example, MAs are mixed to the standard fuel components, or the use of reactor cores dedicated to transmutation in a separate stratum of the fuel cycle.[3,4] In the latter case, the dedicated reactor core should be loaded with MA-dominated fuel, and both critical and subcritical [i.e., accelerator-driven system (ADS)] versions of such cores have been the subject of several studies.[5]

Although the major challenges of the dedicated cores are to be found in the appropriate fuel development and in the demonstration of the viability of the ADS concept, one aspect of particular relevance is the uncertainty assessment of the nominal predicted characteristics of such cores. A first partial intercomparison exercise was performed under the auspices of the Nuclear Energy Agency (NEA) of the Organization for Economic Cooperation and Development[6] (OECD). The published results did show large discrepancies among the different parameters, most probably to be attributed to nuclear data uncertainties. Some other studies[7–9] have been performed that examine specific aspects, but no comprehensive analysis has been performed until now. Also, these studies only partially address the issue of the impact of high-energy ($E > 20$ MeV) data on ADS core performance

*E-mail: massimo.salvatores@cea.fr

†Present address: DEN/DIR Building 101, CEA/Cadarache, F. 13108 St.-Paul-Lez-Durance Cedex, France

assessment. The impact of uncertainties can be very significant, both on the safety assessment and the economic evaluation of a dedicated core. In fact, as an example, uncertainties on the subcriticality level of an ADS dedicated to transmutation induce the need to define design margins, which in turn can result in a proton beam-power requirement that calls for an accelerator able to deliver up to twice as much current of what is needed according to the nominal design value of the subcriticality. Moreover, a sound uncertainty analysis can help to define new priority measurements of specific cross sections in well-defined energy domains, together with target accuracies. In this work, we have performed such an analysis for a representative ADS-dedicated core with U-free, MA-dominated fuel. We have addressed both standard core-related parameters (which will be applicable both to critical or subcritical versions of the core) and high-energy-related parameters (like damages and gas production in the structures) potentially sensitive to data at energies $E > 20$ MeV. An attempt has also been made to define target accuracies and to point out major data needs.

II. UNCERTAINTY ANALYSIS

II.A. Theoretical Background

The principles of uncertainty analysis and its applications to the fission reactor field are well documented.[10] We will simply recall here that we can represent a generic integral reactor parameter Q (such as k_{eff}, or a reactivity coefficient, or even a reaction rate like the neutron-induced damage in the structures) as a function of cross sections:

$$Q = f(\sigma_1, \sigma_2, \ldots, \sigma_J) \ , \tag{1}$$

where $\sigma_1, \sigma_2, \ldots, \sigma_J$ represent cross sections by isotope, type of reaction, and energy range (or energy group, in a multigroup representation). The uncertainties associated with the cross section can be represented in the form of a variance-covariance matrix:

$$C_\sigma = \begin{pmatrix} c_{11} & c_{12} & \ldots & c_{1J} \\ c_{12} & c_{22} & \ldots & c_{2J} \\ \ldots & \ldots & \ldots & \ldots \\ c_{1J} & c_{2J} & \ldots & c_{JJ} \end{pmatrix} \ , \tag{2}$$

where the elements c_{ij} represent the expected values related to the parameters σ_j and σ_i.

The variations of the integral parameter Q due to variations of σ can be expressed using perturbation theories[11] to evaluate sensitivity coefficients S:

$$\delta Q/Q = \sum_j S_j \frac{\delta\sigma_j}{\sigma_j} \ , \tag{3}$$

where the sensitivity coefficients S_j are formally given by

$$S_j = \frac{\partial Q}{\partial \sigma_j} \cdot \frac{\sigma_j}{Q} \ . \tag{4}$$

The variance of Q can then be obtained as

$$\mathrm{var}(Q) = \sum_{j:i}^{J} S_j S_i c_{ij} \ . \tag{5}$$

To exploit Eq. (5) one needs to obtain explicitly the S_j coefficients and to establish an appropriate variance-covariance matrix. For a set of integral parameters Q_n $(n = 1 \ldots N)$, the assessment of the variances as given by Eq. (5) is of course relevant, but it is also relevant to assess the inverse problem, i.e., what are the required data uncertainties to meet specific target accuracies on the Q_n parameter.

The unknown uncertainty data requirements d_i can be obtained solving the following minimization problem[12]:

$$\sum_i \lambda_i / d_i^2 = \min \ , \quad i = 1 \ldots I \tag{6}$$

with the following constraints:

$$\sum_i S_{ni}^2 d_i^2 < Q_n^T \ , \quad n = 1 \ldots N \ , \tag{7}$$

where S_{ni} are the sensitivity coefficients for the integral parameter Q_n, and Q_n^T are the target accuracies on the N integral parameters. The cost parameters λ_i are related to each σ_i and should give a relative figure of merit of the difficulty of improving that parameter (e.g., reducing uncertainties with an appropriate experiment).

II.B. Sensitivity Coefficients and Perturbation Theories

For practical purposes, we will distinguish the explicit dependence from some cross sections (e.g., σ_i^e) and the implicit dependence from some other cross sections (e.g., σ_j^{im}) in the general expression of any integral parameter Q:

$$Q = f(\sigma_j^{im}, \sigma_i^e) \ . \tag{8}$$

As an example, we consider a reaction rate

$$R = \langle \underline{\sigma}^e, \underline{\Phi} \rangle \tag{9}$$

where brackets $\langle \, , \rangle$ indicate integration over the phase space. Note that in the present analysis, $\underline{\Phi}$ is the inhomogeneous flux driven by the external source. It would be the homogeneous flux in the case of critical core studies. Instead, the adjoint flux that appears later in the paper corresponds to the homogeneous calculation in all cases. In Eq. (9), $\underline{\sigma}^e$ can be an energy-dependent detector cross section; R is explicitly dependent on the $\underline{\sigma}^e$ and

implicitly dependent on the cross sections that characterize the system, described by the flux $\underline{\Phi}$. In other terms, R depends on the system cross sections via $\underline{\Phi}$. Equation (3) can be rewritten as follows:

$$\delta Q/Q = \sum_j S_j \frac{\delta\sigma_j^{im}}{\sigma_j^{im}} + \left(\frac{\partial Q}{\partial \sigma^e}\cdot\frac{\sigma^e}{Q}\right)\cdot\frac{\delta\sigma^e}{\sigma^e} \ , \qquad (10)$$

where we have the hypothesis of an explicit dependence of Q on only one σ^e. If we drop the index *im*,

$$\delta Q/Q = \sum_j S_j \frac{\delta\sigma_j}{\sigma_j} + \left(\frac{\partial Q}{\partial \sigma^e}\cdot\frac{\sigma^e}{Q}\right)\cdot\frac{\delta\sigma^e}{\sigma^e} = I + D \ , \qquad (11)$$

where the term I is generally called the indirect effect, and the term D is called the direct effect. While the direct effects can be obtained with explicit expressions of the derivatives of Q, the indirect effect (i.e., the sensitivity coefficients S) can be obtained with perturbation expression, most frequently at the first order.[11]

In what follows, we will recall in a simplified way the formulations of the sensitivity coefficients at the first order for the indirect effects related to reactivity coefficients,[13] reaction rates,[11] and nuclide transmutation (i.e., evolution in time[14]). Reactivity loss during irradiation will also be treated as well as the cases of effective fraction of delayed neutrons and of the decay heat.

II.B.1. Reactivity Coefficients

A reactivity coefficient (like the Doppler effect) can be expressed as a variation of the reactivity of the unperturbed system (characterized by a value K of the multiplication factor, a Boltzmann operator M, a flux $\underline{\Phi}$, and an adjoint flux $\underline{\Phi}^*$):

$$\Delta\rho = \left(1 - \frac{1}{K_p}\right) - \left(1 - \frac{1}{K}\right) = \frac{1}{K} - \frac{1}{K_p} \ , \qquad (12)$$

where K_p corresponds to a variation of the Boltzmann operator such that

$$M \to M_p(= M + \delta M_p) \qquad \underline{\Phi} \to \underline{\Phi}_p(=\underline{\Phi} + \delta\underline{\Phi}_p)$$
$$\underline{\Phi}^* \to \underline{\Phi}_p^*(= \underline{\Phi}^* + \delta\underline{\Phi}_p^*) \qquad K \to K_p(=K + \delta K_p) \ . \qquad (13)$$

The sensitivity coefficients (at first order) for $\Delta\rho$ to variations of the σ_j are given as in Ref. 13:

$$S_j^{RO} = \frac{\partial(\Delta\rho)}{\partial\sigma_j}\cdot\frac{\sigma_j}{\Delta\rho} = \left\{\frac{1}{I_f^p}\langle\underline{\Phi}_p^*, \sigma_j\underline{\Phi}_p\rangle - \frac{1}{I_f}\langle\underline{\Phi}^*, \sigma_j\underline{\Phi}\rangle\right\} \ , \qquad (14)$$

where $I_f = \langle\underline{\Phi}^*, F\underline{\Phi}\rangle$ and $I_f^p = \langle\underline{\Phi}_p^*, F\underline{\Phi}_p\rangle$, F being the neutron fission production part of the M $(= F - A)$ operator.

II.B.2. Reaction Rates

The classical formulations found in Ref. 11, for example, can be applied to the case of damage rate or He production in the structures or to the power peak factor in the core:

$$R = \langle\underline{\Phi}, \underline{\Sigma}_R\rangle \ . \qquad (15)$$

The sensitivity coefficients are given by

$$S_j^R = \langle\underline{\Psi}_R^*, \sigma_j\underline{\Phi}\rangle \ , \qquad (16)$$

where $\underline{\Phi}$ is as defined previously, $\underline{\Psi}_R^*$ is the solution of

$$M^*\underline{\Psi}_R^* = \underline{\Sigma}_R \ , \qquad (17)$$

and M^* is the adjoint of the operator M.

II.B.3. Nuclide Transmutation

The generic nuclide K transmutation during irradiation can be represented as the nuclide density variation between time t_0 and t_F. If we denote n_F^K the final density, the appropriate sensitivity coefficient is given by

$$S_j^K = \frac{\partial n_F^K}{\partial\sigma_j}\cdot\frac{\sigma_j}{n_F^K} = \frac{1}{n_F^K}\int_{t_0}^{t_F}\underline{n}^*\sigma_j\underline{n}\,dt \ , \qquad (18)$$

where the time-dependent equations to obtain $\underline{n}^*$ and $\underline{n}$, together with their boundary conditions, are defined in Ref. 14.

The method previously described does not take into account the coupling with the flux field,[15,16] neglecting in this way the feedback from flux and spectrum changes during irradiation time. We show in Sec. IV.F that this approximation is acceptable in the cases under study and that the time dependence of the flux spectrum is negligible.

II.B.4. Reactivity Loss During Irradiation, $\Delta\rho^{cycle}$

At the first order, and neglecting the cross-section variation during irradiation (which is a good approximation for fast neutron systems), we can write

$$\Delta\rho^{cycle} = \sum_K \Delta n^K\rho_K \ , \qquad (19)$$

where

$$\Delta n^K = n_F^K - n_0^K \qquad (20)$$

and ρ_K is the reactivity per unit mass associated with isotope K.

The related sensitivity coefficients S_j^{cycle} associated with the variation of an σ_j are given by

$$S_j^{cycle} = \frac{\sigma_j}{\Delta\rho^{cycle}} \frac{\partial \Delta\rho^{cycle}}{\partial \sigma_j} = \frac{\sigma_j}{\Delta\rho^{cycle}} \left(\sum_K \frac{\partial n^K}{\partial \sigma_j} \cdot \rho_K + \sum_K \Delta n^K \frac{\partial \rho_K}{\partial \sigma_j} \right) . \quad (21)$$

Using the formulations of Secs. II.B.1 and II.B.3, we obtain

$$S_j^{cycle} = \sum_K \frac{\rho_K}{\Delta\rho^{cycle}} \int_{t_0}^{t_F} \underline{n}^* \sigma_j \underline{n} \, dt + \left\{ \frac{1}{I_f^p} \langle \underline{\Phi}_p^*, \sigma_j \underline{\Phi}_p \rangle - \frac{1}{I_f} \langle \underline{\Phi}^*, \sigma_j \underline{\Phi} \rangle \right\} , \quad (22)$$

where the index p refers to the core state at $t = t_F$.

Also in this case, the time-dependent variation of the flux spectrum during irradiation is supposed to be of negligible impact on the sensitivity coefficients for $\Delta\rho^{cycle}$ (see Sec. IV.F).

II.B.5. The φ^* Parameter

The φ^* parameter is defined for an external source-driven system as the ratio of the average external source importance to averaged fission neutron importance:

$$\varphi^* = \frac{\langle \underline{\Phi}^* S \rangle}{\langle S \rangle} \Big/ \frac{\langle \underline{\Phi}^*, F\underline{\Phi} \rangle}{\langle F\underline{\Phi} \rangle} = \left(\frac{1}{k_{eff}} - 1 \right) \Big/ \left(\frac{1}{K_S} - 1 \right) , \quad (23)$$

where

$$k_{eff} = \frac{\langle \underline{\Phi}^*, F\underline{\Phi} \rangle}{\langle \underline{\Phi}^*, A\underline{\Phi} \rangle}$$

$$K_S = \frac{\langle F\underline{\Phi} \rangle}{\langle A\underline{\Phi} \rangle}$$

$\underline{\Phi}$ = solution of the inhomogeneous equation with external source S:

$$A\underline{\Phi} = F\underline{\Phi} + S . \quad (24)$$

Equation (23) is a special case of a real and adjoint flux functional ratio I_S for which a generalized perturbation theory (GPT) has also been established.[9]

For that case, the sensitivity coefficients are given by

$$S_j^{\varphi^*} = \frac{\partial \varphi^*}{\partial \sigma_j} \frac{\sigma_j}{\varphi^*} = \frac{\sigma_j}{\varphi^*} \{ \langle \underline{\Psi}^*, \sigma_j \underline{\Phi} \rangle + \langle \underline{\Psi}, \sigma_j \underline{\Phi}^* \rangle \} , \quad (25)$$

where $\underline{\Psi}^*$ and $\underline{\Psi}$ (generalized importance functions) are the solution of the following equations:

$$M^* \underline{\Psi}^* = - \frac{\nu\Sigma_f(r,E) \langle \underline{\Phi}^*, \underline{\chi} \rangle}{\langle \underline{\Phi}^*, F\underline{\Phi} \rangle} + \frac{\nu\Sigma_f(r,E)}{\langle F\underline{\Phi} \rangle} \quad (26)$$

and

$$M\underline{\Psi} = \frac{S(r,E)}{\langle \underline{\Phi}^* S \rangle} - \frac{\chi(E) \langle \underline{\nu\Sigma}_f \underline{\Phi} \rangle}{\langle \underline{\Phi}^*, F\underline{\Phi} \rangle} , \quad (27)$$

where we have explicitly introduced the energy- and space-dependent form of the fission operator, and $\nu\Sigma_f(E,r)$ (component of the vector $\underline{\nu\Sigma}_f$) is the macroscopic fission cross section multiplied by the prompt neutron fraction at energy E and space point r, and $\chi(E)$ (component of the vector $\underline{\chi}$) is the fraction of the fission spectrum at energy E; the brackets $\langle , \rangle$ indicate integration over energy and space.

II.B.6. Decay Heat

The decay heat is defined as

$$H(t) = \sum_K \lambda_K Q_K n^K(t) , \quad (28)$$

where for each isotope K, λ_K are the decay constants, Q_K is the heat released in decay reaction, and $n_K(t)$ are the nuclide densities at time t. The equations for $n_K(t)$ are the classical ones:

$$\frac{dn^K(t)}{dt} = \sum_F \gamma_{K,f} \tau_f + \sum_j n_K^j(t) \tau_j b_{j\to K} + \sum_i n^i(t) \lambda_i b_{i\to K} - \tau_K n^K(t) - \lambda_K n^K(t) , \quad (29)$$

or in a more compact form,

$$\frac{dn^k(t)}{dt} = b_k + \sum_{j=1}^{K-1} C_{kj} n^j(t) - C_{kk} n^k(t) , \quad (30)$$

where

$\gamma_{K,f}$ = fission yields for fissionable isotope f

τ = microscopic reaction rates

$b_{j\to k}$ = branching ratios.

This is an inhomogeneous Bateman-type equation that defines the appropriate nuclide field. The uncertainty on $H(t)$ is obtained by combining the appropriate derivatives of H with respect to λ, Q, and n and accounting for possible correlations. As far as variations of the n_K terms, they can be evaluated using the perturbation techniques indicated in Sec. II.B.3. A specific feature is represented by the variation of the fission yields γ, i.e., by the variation of the source term b_K in Eq. (30).

The relative sensitivity coefficients corresponding to the decay heat at $t = t_x$ are given by

$$S^{\gamma}_{K,f} = \tau_f \frac{\partial n^K_{t=t_x}}{\partial \gamma_{K,f}} \cdot \frac{\gamma_{K,f}}{n^K_{t=t_x}} = \frac{\tau_f}{n^K_{t=t_x}} \int_0^{t_x} \underline{n}^* \gamma_{K,f}\, dt \ . \quad (31)$$

II.B.7. The Effective Fraction of Delayed Neutrons

The effective fraction of delayed neutrons, $\hat{\beta}_{eff}$, is defined by the following equation:

$$\hat{\beta}_{eff} = \sum_m \hat{\beta}^m_{eff} \ , \quad (32)$$

where $\hat{\beta}^m_{eff}$ is the effective delayed-neutron fraction of fissile material m. For each fissile material m, $\hat{\beta}_{eff} = \sum_i \hat{\beta}_i$, where $\hat{\beta}_i$, the effective fraction for the precursor group i, is expressed as follows:

$$\hat{\beta}_i = \frac{\langle \chi^d_i \underline{\Phi}^*, \beta_i \nu^d \Sigma_f \underline{\Phi} \rangle}{\langle \underline{\Phi}^*, F \underline{\Phi} \rangle}$$

$$= \frac{\beta_i \int [\chi^d_i(E) \Phi^*(r,E,\Omega)][\nu^d(E') \Sigma_f(r,E') \Phi(r,E',\Omega')]\, dr}{\langle \underline{\Phi}^*, F \underline{\Phi} \rangle} \ , \quad (33)$$

where

ν^d = number of delayed neutrons emitted by fission

χ^d_i = delayed-neutron spectrum for the group i

β_i = fraction of delayed neutrons from the group i.

Using the GPT, the sensitivity coefficients for $\hat{\beta}_{eff}$, including both the direct (i.e., related to the delayed-neutron parameters) and the indirect effect, are given by

$$S^{\hat{\beta}}_j = \frac{\partial \hat{\beta}_{eff}}{\partial \beta_i} \frac{\beta_i}{\hat{\beta}_{eff}} + \frac{\partial \hat{\beta}_{eff}}{\partial \chi^d_i} \frac{\chi^d_i}{\hat{\beta}_{eff}} + \frac{\partial \hat{\beta}_{eff}}{\partial \sigma_j} \frac{\sigma_j}{\hat{\beta}_{eff}}$$

$$= \frac{\partial \hat{\beta}_{eff}}{\partial \beta_i} \frac{\beta_i}{\hat{\beta}_{eff}} + \frac{\partial \hat{\beta}_{eff}}{\partial \chi^d_i} \frac{\chi^d_i}{\hat{\beta}_{eff}} + \frac{\sigma_j}{\hat{\beta}_{eff}}$$

$$\times \{ \langle \underline{\Psi}^*, \sigma_j \underline{\Phi} \rangle + \langle \underline{\Psi}, \sigma_j \underline{\Phi}^* \rangle \} \ , \quad (34)$$

where Ψ^* and $\underline{\Psi}$ (generalized importance functions) are the solutions of the following equations:

$$(A^* - F^*) \underline{\Psi}^* = \frac{\beta_i [\underline{\Phi}^* \chi^d_i] \nu^d \Sigma_f(r,E)}{\langle \chi^d_i \underline{\Phi}^*, \beta_i \nu^d \Sigma_f \underline{\Phi} \rangle} - \frac{[\underline{\Phi}^* \chi] \nu \Sigma_f(r,E)}{\langle \Phi^*, F \underline{\Phi} \rangle} \quad (35)$$

and

$$\left(A - \frac{1}{K} F \right) \underline{\Psi} = \frac{[\beta_i \nu^d \Sigma_f \underline{\Phi}] \chi^d_i(E)}{\langle \chi^d_i \underline{\Phi}^*, \beta_i \nu^d \Sigma_f \underline{\Phi} \rangle} - \frac{[\nu \Sigma_f \underline{\Phi}] \chi}{\langle \underline{\Phi}^*, F \underline{\Phi} \rangle} \ . \quad (36)$$

II.C. Calculational Tools and Basic Data Library

All the sensitivity calculations have been performed with the ERANOS code system,[17] which allows us to calculate homogeneous and inhomogeneous solutions of the Boltzmann equation, generalized importance functions, and to perform perturbation and uncertainty analysis. The discrete ordinate module BISTRO (Ref. 18) has been used to perform flux and generalized importance function calculations. An $S_4 P_1$ approximation in RZ geometry has been proved accurate enough for this type of calculation.

Decay heat calculations have been performed with the ORIGEN code.[19]

Cross-section data have been processed to the required multigroup structure, starting from the JEF-2.2 data files.[20] Homogeneous cross sections have been calculated because heterogeneity effects on the cross sections are rather small in these hard neutron spectra. Delayed-neutron data were also taken from the JEF-2.2 files.

The basic multigroup structure (33 energy groups, see, for example, Table XI) has an upper energy limit at 19.64 MeV.

To investigate high-energy ($E > 20$ MeV) effects in a subcritical system driven by a spallation neutron source induced by high-energy protons ($E_p \approx 1$ GeV), the multigroup data have been extended up to 150 MeV using the data provided in Ref. 21. For that purpose, ten energy groups with a lethargy width of 0.2 have been added to the basic 33-energy-group structure to cover the energy range from 19.64 to 150 MeV.

III. THE REFERENCE DEDICATED SYSTEM FOR THE UNCERTAINTY ANALYSIS

III.A. The Reference System

The methodology outlined in Sec. II has been applied to a dedicated system that has some general features (e.g., the mass ratio between plutonium and MA, the americium-to-curium ratio, etc.) that are representative of the class of MA transmuters with a fast neutron spectrum and a fertile-free fuel, as proposed, for example, in the framework of the OMEGA project in Japan, as studied at Commissariat à l'Energie Atomique, France, or examined in the United States.

The target and the coolant material of the core are the Pb-Bi eutectic. This is a more specific choice, in

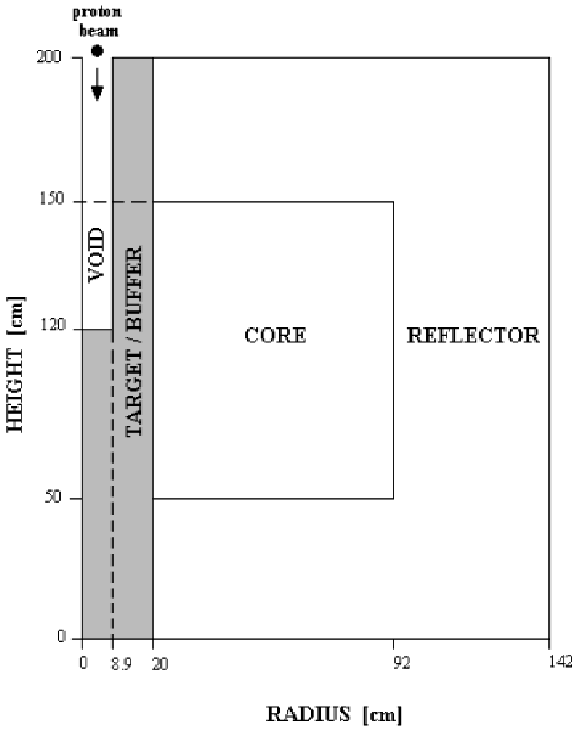

Fig. 1. Geometry of the reference ADS core (R, Z model).

particular in terms of coolant, which in principle, however, does not affect much the overall uncertainty analysis features because these are more related to the type of neutron spectrum (i.e., fast versus thermal neutron spectrum). Finally, the system that we have chosen is very close to the subcritical core, which has been analyzed in the framework of an OECD-NEA benchmark.[6] The geometric model and compositions are given in Fig. 1 and Table I, respectively.

The spallation source in space and energy has been generated using the MCNPX code, assuming a beam radius of 10 cm of protons with an energy of 1 GeV. For the successive propagation of neutrons using the deterministic code system indicated in Sec. II.C, a cut-off energy of 20 MeV has been chosen. As far as the spectral distribution, 14% of the spallation neutron source is above 20 MeV. Figures 2 and 3 show the axial and radial distributions, respectively, of the neutron source split into four energy bins: 0 to 6.1, 6.1 to 19.6, 19.6 to 55.2, and 55.2 to 150 MeV.

III.B. Main Parameters of the Reference System

The main parameters of the reference system, obtained with the calculation route indicated in Secs. II.C

TABLE I

Compositions of the Reference Core

Fuel				Reflector		Target/Buffer	
Isotope	Compositions (10^{24} at./cm^3)	Isotope	Compositions (10^{24} at./cm^3)	Isotope	Compositions (10^{24} at./cm^3)	Isotope	Compositions (10^{24} at./cm^3)
^{237}Np	4.377E−04[a]	^{58}Fe	4.386E−05	^{54}Fe	2.990E−03	Pb	1.320E−02
^{238}Pu	4.226E−05	^{50}Cr	1.128E−04	^{56}Fe	4.560E−02	Bi	1.632E−02
^{239}Pu	5.051E−04	^{52}Cr	2.096E−03	^{57}Fe	1.075E−03		
^{240}Pu	2.321E−04	^{53}Cr	2.328E−04	^{58}Fe	1.344E−04		
^{241}Pu	1.232E−04	^{54}Cr	5.682E−05	^{50}Cr	3.458E−04		
^{242}Pu	9.102E−05	^{58}Ni	6.451E−05	^{52}Cr	6.422E−03		
^{241}Am	8.084E−04	^{60}Ni	2.384E−05	^{53}Cr	7.134E−04		
^{242m}Am	1.089E−05	^{61}Ni	1.015E−06	^{54}Cr	1.741E−04		
^{243}Am	5.827E−04	^{62}Ni	3.173E−06	^{58}Ni	1.977E−04		
^{242}Cm	4.079E−08	^{64}Ni	7.792E−07	^{60}Ni	7.305E−05		
^{243}Cm	3.326E−06	Mo	1.163E−04	^{61}Ni	3.111E−06		
^{244}Cm	2.371E−04	Mn	1.114E−04	^{62}Ni	9.724E−06		
^{245}Cm	3.164E−05	Pb	6.360E−03	^{64}Ni	2.388E−06		
^{246}Cm	5.355E−07	Bi	7.865E−03	Mo	3.565E−04		
Zr	7.477E−03	^{182}W	6.984E−06	Mn	3.412E−04		
^{15}N	1.058E−02	^{183}W	3.770E−06	Pb	4.075E−03		
^{54}Fe	9.759E−04	^{184}W	8.045E−06	Bi	5.039E−03		
^{56}Fe	1.488E−02	^{186}W	7.439E−06	^{182}W	2.140E−05		
^{57}Fe	3.507E−04			^{183}W	1.155E−05		
				^{184}W	2.465E−05		
				^{186}W	2.280E−05		

[a]Read as 4.377×10^{-4}.

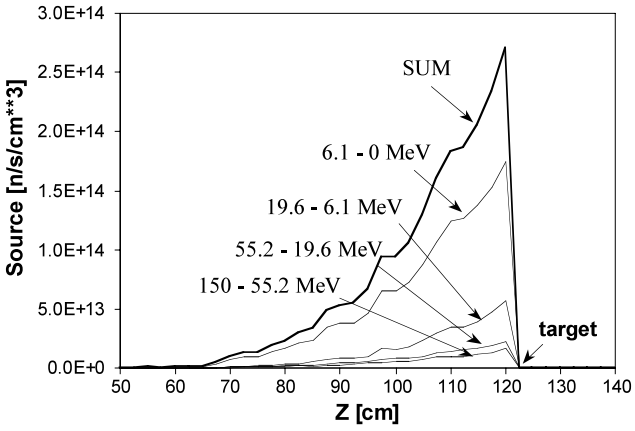

Fig. 2. Axial distribution of the neutron source by energy domain (MCNPX calculation).

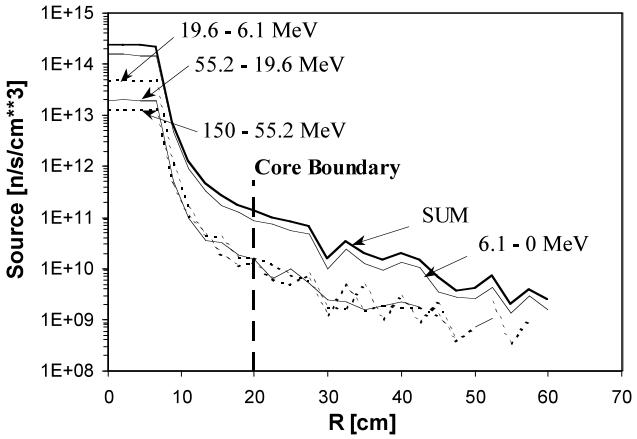

Fig. 3. Radial distribution of the neutron source by energy domain (MCNPX calculation).

TABLE II

Main Parameters of the Reference System

k_{eff}	$\hat{\beta}_{eff}$ (pcm)	$\Delta\rho^{Doppler}$ [a]	$\Delta\rho^{void}$	$\Delta\rho^{cycle}$ 1 yr [b]	$\Delta\rho^{cycle}$ 2 yr [b]	Decay Heat [c]	Peak Power [d]
0.948164	185.4	−0.00026	+0.02906	−0.01196	−0.02158	25 MW(thermal)	2.9

$(\Delta n/n)^{cycle}$ [e] $[10^{24}$ at./cm$^3]$						
^{238}Pu	^{241}Am	^{242m}Am	^{243}Am	^{242}Cm	^{244}Cm	^{245}Cm
1.23	−1.07E−1 [f]	7.66E−1	−8.99E−2	6.57E+2	9.62E−2	4.74E−2

[a]For $\Delta T = T - T_{Ref} = 1773$ to 980 K.
[b]At full power.
[c] At discharge. Nominal power of the core: 377 MW(thermal).
[d]See text.
[e]$(n_F - n_0)/n_0$ after 1 yr irradiation.
[f]Read as -1.07×10^{-1}.

TABLE III

Main Parameters of the Reference System

φ^*	Maximum dpa[a] ($s^{-1} \times cm^{-3}$)	Maximum He Production[a] ($s^{-1} \times cm^{-3}$)	Maximum H Production[a] ($s^{-1} \times cm^{-3}$)	Maximum (He production)/dpa[a]
1.18	2.58E+16[b]	6.15E+15	6.77E+16	0.24

[a]See text for description.
[b]Read as 2.58×10^{16}.

and III.A using the 33-energy-group structure, with upper energy boundary at 19.64 MeV, are given in Tables II and III.

In Table III, φ^* is the ratio of the average external source importance to average fission neutron importance introduced previously.

The peak power is defined as the point maximum power value normalized to the total power. Max dpa, Max He production, Max H production are the values of the displacements per atom (dpa), He production, and H production (all in iron) at the spatial point where they reach their maximum value. The maximum value of the ratio (He production)/dpa is calculated at its own

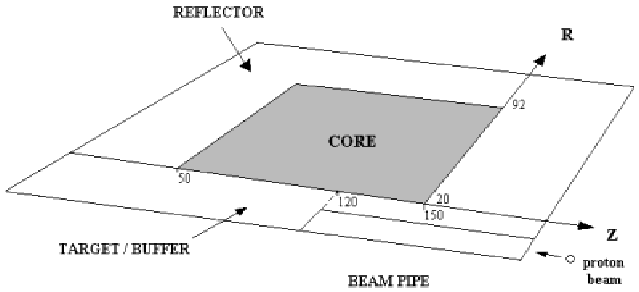

Fig. 4a. Reference coordinates for the fuel region.

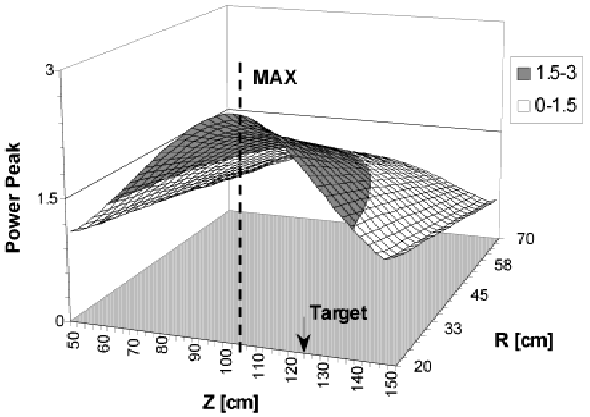

Fig. 4b. Maximum peak power: $(R, Z) = (20\text{ cm}, 102.5\text{ cm})$.

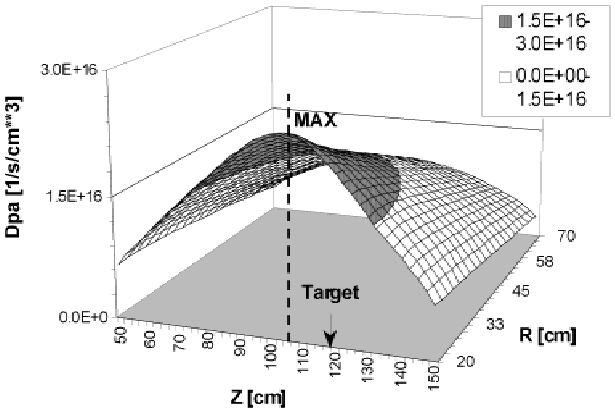

Fig. 4c. Maximum dpa: $(R, Z) = (20\text{ cm}, 105\text{ cm})$.

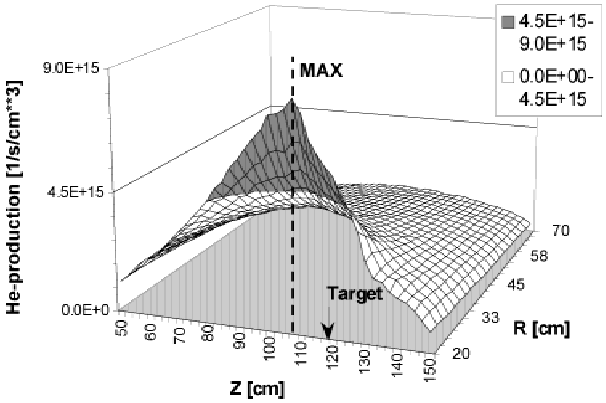

Fig. 4d. Maximum He production: $(R, Z) = (20\text{ cm}, 107.5\text{ cm})$.

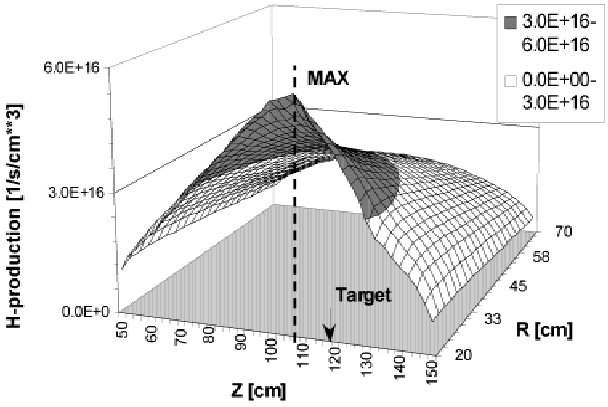

Fig. 4e. Maximum H production: $(R, Z) = (20\text{ cm}, 107.5\text{ cm})$.

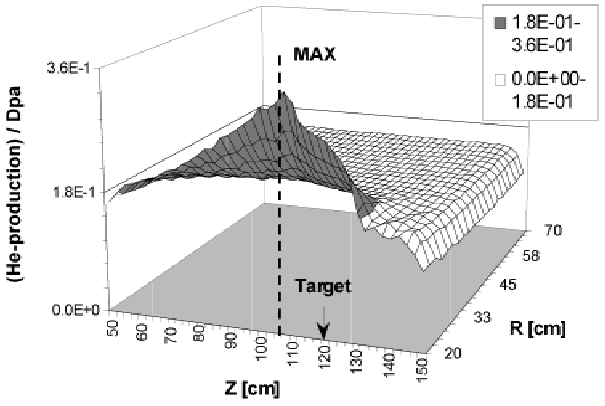

Fig. 4f. Maximum (He Production)/dpa: $(R, Z) = (20\text{ cm}, 107.5\text{ cm})$.

maximum value position. In Figs. 4b through 4f, the spatial distributions of the peak power, Max dpa, Max He production, Max H production, and Max (He production)/dpa are shown (Fig. 4a allows visualization of the reference coordinate system).

One can observe that the power peak is obtained approximately at core midplane, where the flux reaches its highest value. The Max dpa, He-, and H production are located a few centimetres above the core midplane, the location of the maximum of the higher energy neutrons coming from spallation. The He- and H-production spatial distribution are peaked at the core/buffer interface, while the dpa and power are more evenly distributed in the core.

In Table II, $\Delta\rho^{\text{Doppler}}$ corresponds to the reactivity induced by a jump in temperature between 980 and 1773 K. The $\Delta\rho^{cycle}$ is the reactivity variation resulting from a 1- or 2-yr irradiation. A more detailed analysis of these parameters is given later in this paper.

Finally, the $(\Delta n/n)^{cycle}$, i.e., the relative variation of a few selected major isotope nuclear densities (^{238}Pu, ^{241}Am, ^{242m}Am, ^{243}Am, ^{242}Cm, ^{244}Cm, and ^{245}Cm), is a measure of the effectiveness of the transmutation process.

In Figs. 5 and 6, the neutron flux and adjoint spectra are also given. One can observe a harder neutron spectrum (both real and adjoint) with respect to a standard fast reactor (e.g., for the PHENIX reactor). This effect is related partly to the contribution of the high-energy neutrons coming from spallation, partly to the presence of Pb-Bi as coolant, and partly to the higher importance of the high-energy fissions in the system. It can be of interest in this respect to inspect the energy shape of the $\eta = \nu\sigma_f/\sigma_a$ parameter for several actinides. In fact, the sharp high-energy slope of the η of ^{241}Am, ^{243}Am, and ^{244}Cm (present in high percentage in our reference system) shows a remarkable difference with respect to that of ^{239}Pu, for example (see Fig. 7).

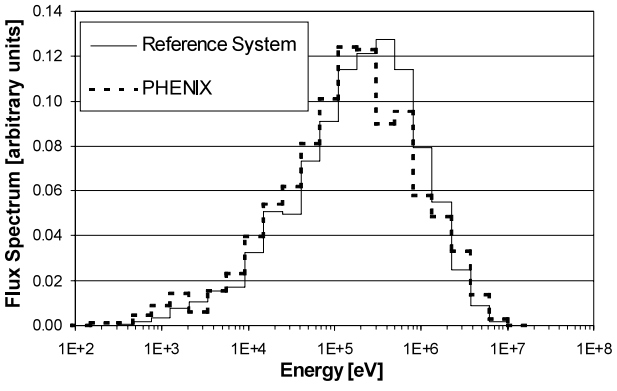

Fig. 5. Core average flux spectrum. For comparison, the flux spectrum for the typical fast reactor PHENIX is also shown.

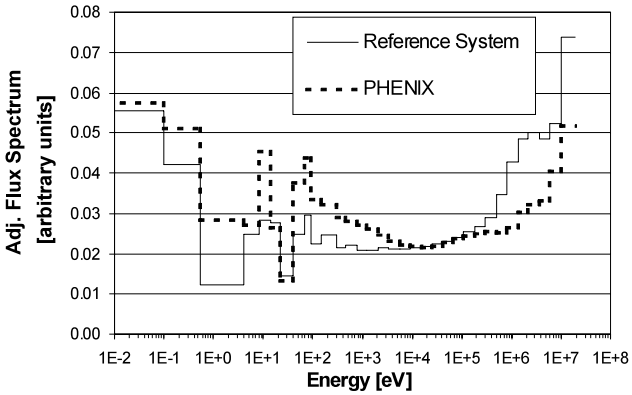

Fig. 6. Core average adjoint flux spectrum. For comparison, the adjoint flux spectrum for the typical fast reactor PHENIX is also shown.

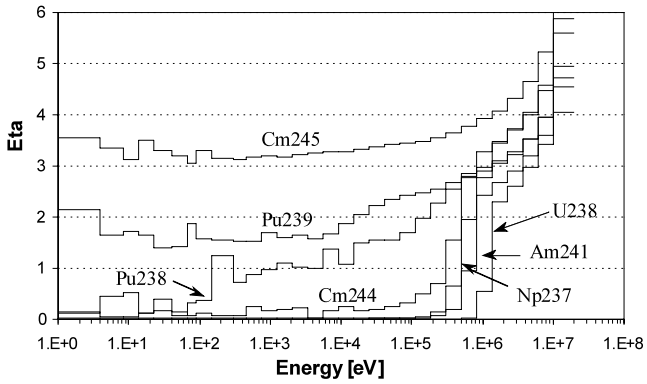

Fig. 7. The $\eta = \nu\sigma_f/\sigma_a$ energy shape for selected actinides.

IV. UNCERTAINTY ANALYSIS

IV.A. Variance-Covariance Matrix for Multigroup Data

Variance-covariance data are still scarce in all major data files, in particular for minor actinides and materials like Pb or Bi, which play an important role in our study. Since a significant part of our work was based on the JEF library data, we have used for major actinides and some structural material (Fe, Cr, Ni) uncertainty data provided in Ref. 22. For major actinides, since most evaluations in the major data files are based on common sets of experimental data, significant variation of the uncertainty values is not expected. For minor actinides, we have defined uncertainties based on a comparative analysis among major data files performed in the framework of the Nuclear Science Committee of the NEA of OECD (Ref. 23). For example, large uncertainties for thermal and epithermal data of ^{241}Am or ^{243}Am have been pointed out in this study. For structural materials like Pb and Bi,

we have intercompared data files and extracted an educated guess for uncertainties.

The diagonal values used, reduced to a 15-energy-group substructure of the reference 33-group structure, are shown in Tables IV, V, and VI.

As far as correlations, most of our analysis has been based on the hypothesis of no correlation among uncertainties, in particular of no energy correlation for a specific reaction type. Since the present analysis is performed at 15 energy groups, it implicitly allows for a full energy correlation for each reaction type within the energy range of each group.

As mentioned previously, the variance-covariance data are relatively seldom associated with evaluated data files, and in particular data for MAs have not been assessed. However, it was considered of interest to allow for some hypothesis, at least on the energy correlations, to gain some insight on their potential impact. We have chosen rather arbitrarily to introduce a full correlation on selected energy domains, the same for all types of cross sections and isotopes. These energy ranges are 20 to 1 MeV, 1 MeV to 100 keV, 100 keV to 1 keV, and 1 keV down to epithermal energy. The purpose of these correlations is essentially to impose energy shapes on the cross sections, as obtained, for example, from model calculations. We refer to uncertainties obtained with this hypothesis as having been obtained with partial energy correlations (PECs). The uncertainty analysis presented

TABLE IV

Variance Matrix for Major Actinides*

Group	(MeV)[a]	ν	σ_f	σ_{inel}	σ_{el}	σ_{capt}	$\sigma_{n,2n}$	ν	σ_f	σ_{inel}	σ_{el}	σ_{capt}	$\sigma_{n,2n}$
		^{238}Pu and ^{240}Pu						^{239}Pu					
1	19.6	0.012	0.05	0.15	↑	0.3	0.16	0.008	0.03	0.1	↑	0.1	0.13
2	6.07	0.014	0.05	0.15		0.3		0.0075	0.037	0.1		0.085	0.25
3	2.23	0.018	0.1	0.15		0.3		0.007	0.037	0.1		0.095	
4	1.35	0.02	0.1	0.15		0.3		0.0065	0.065	0.15		0.13	
5	4.98E−1[b]	0.028	↑	0.2		0.25		0.0055	0.04	0.15		0.13	
6	1.83E−1	0.03		0.2		0.15		0.008	0.028	0.15		0.078	
7	6.74E−2	0.0312		0.2	0.1	0.1		0.015	0.03	0.2		0.039	
8	2.48E−2	0.0311				0.1		0.008	0.045	0.25	0.05	0.056	
9	9.12E−3	0.031	0.2			0.1		0.008	0.063	0.25		0.056	
10	2.04E−3	0.03				0.1		0.0051	0.02			0.065	
11	4.54E−4	0.029				0.1		0.005	0.025			0.065	
12	2.26E−5	0.028				0.08		0.003	0.025			0.065	
13	4.00E−6	0.027	↓		↓	0.03		0.0024	0.025			0.039	
14	5.40E−7	0.026	0.5		0.05	0.005		0.0022	0.0025			0.008	
15	1.00E−7	0.019	0.5		0.05	0.005		0.002	0.0025		↓	0.008	
		^{241}Pu						^{242}Pu					
1	19.6	0.01	0.125	0.15	↑	0.5	0.18	0.012	0.05	0.15	↑	0.3	0.25
2	6.07	0.0095	0.2	0.15		0.5	0.2	0.015	0.05	0.15		0.3	
3	2.23	0.009	0.05	0.15		0.4		0.019	0.1	0.15		0.3	
4	1.35	0.0085	0.05	0.15		0.3		0.02	0.1	0.15		0.3	
5	4.98E−1	0.008	0.06	0.2		0.2		0.03	↑	0.2		0.25	
6	1.83E−1	0.007	0.1	0.2		0.2		0.0317		0.2		0.15	
7	6.74E−2	0.0065	0.1	0.2		0.15		0.0316		0.2	0.1	0.1	
8	2.48E−2	0.006	0.08		0.1	0.15		0.0315				0.1	
9	9.12E−3	0.0055	0.08			0.1		0.031	0.2			0.1	
10	2.04E−3	0.005	0.03			0.1		0.03				0.1	
11	4.54E−4	0.0045	0.03			0.1		0.029				0.09	
12	2.26E−5	0.004	0.03			0.1		0.028				0.08	
13	4.00E−6	0.0035	0.03			0.1		0.027	↓		↓	0.08	
14	5.40E−7	0.003	0.006			0.014		0.025	0.05		0.07	0.01	
15	1.00E−7	0.0024	0.006		↓	0.014		0.02	0.05		0.07	0.01	

*Variance matrix ($\delta\sigma/\sigma$).

[a]Upper energy boundary.

[b]Read as 4.9×10^{-1}.

TABLE V

Variance Matrix for Minor Actinides*

Group[a]	ν	σ_f	σ_{inel}	σ_{el}	σ_{capt}	ν	σ_f	σ_{inel}	σ_{el}	σ_{capt}	ν	σ_f	σ_{inel}	σ_{el}	σ_{capt}
	^{237}Np					^{241}Am and ^{243}Am					^{242m}Am				
1 and 2	0.05	0.25	0.5	0.05	0.4	0.05	0.2	0.5	0.05	0.4	0.05	0.2	0.5	0.05	0.4
3 through 6	0.05	0.25	0.5	0.05	0.15	0.05	0.2	0.5	0.05	0.4	0.05	0.2	0.5	0.05	0.4
7 through 15	0.05	0.25	0.5	0.05	0.15	0.05	0.2	0.5	0.05	0.2	0.05	0.2	0.5	0.05	0.04
	^{242}Cm,^{243}Cm,^{245}Cm,^{246}Cm					^{244}Cm									
1 through 4	0.05	0.3	0.5	0.05	0.4	0.05	0.4	0.5	0.05	0.4					
5 through 13	0.05	0.3	0.5	0.05	0.4	0.05	0.3	0.5	0.05	0.4					
14 and 15	0.05	0.3	0.5	0.05	0.04	0.05	0.3	0.5	0.05	0.04					

*Variance matrix $(\delta\sigma/\sigma)$.
[a]See energy boundary in Table IV.

in Secs. IV and V is based on the no-correlation hypothesis. Section VI summarizes the results obtained with the PEC hypothesis. No correlations have been introduced among isotopes or cross-section types. This is certainly not satisfactory, because cross-section measurements and evaluations account for normalizations, for example, to standard cross sections. However, these correlations, in particular for MAs, have been not

TABLE VI

Variance Matrix for Structural Materials*

Group	(MeV)[b]	^{56}Fe and ^{57}Fe[a]			^{52}Cr[a]			^{58}Ni[a]			Zr		
		σ_{inel}	σ_{el}	σ_{capt}	σ_{inel}	σ_{el}	σ_{capt}	σ_{inel}	σ_{el}	σ_{capt}	σ_{inel}	σ_{el}	σ_{capt}
1	19.6	0.062	0.1	0.15	0.41	0.075	0.15	0.18	0.075	0.14	↑	0.1	0.15
2	6.07	0.068	0.1	0.1	0.06	0.04	0.18	0.14	0.2	0.085		0.1	0.1
3	2.23	0.056	0.1	0.07	0.085	0.025	0.2	0.18	0.17	0.12		0.1	0.07
4	1.35	0.2	0.1	0.07	0.15	0.12	0.17	0.18	0.1	0.09		0.1	0.07
5	4.98E−1[c]		0.08	0.07	0.09	0.15	0.1	0.16	0.04	0.09		0.08	0.07
6	1.83E−1		0.06	0.076		0.15	0.1	0.16	0.04	0.09	0.3	0.06	0.076
7	6.74E−2		↑	0.08		0.15	0.1		0.04	0.09		0.04	0.08
8 and 9				0.08		0.15	0.1		0.04	0.125		0.04	0.08
10 and 11			0.04	0.08		0.15	0.1		0.04	0.11		0.04	0.08
12 and 13			↓	0.08		0.15	0.1		0.04	0.1		0.04	0.08
14 and 15				0.054		0.04	0.079		0.04	0.054	↓	0.04	0.054

Group[b]	^{15}N			Pb and Bi			
	σ_{inel}	σ_{el}	σ_{capt}	σ_{inel}	σ_{el}	σ_{capt}	$\sigma_{n,2n}$
1 and 2	0.4	0.05	0.3	0.4	0.2	0.2	1
2 through 13		0.05	0.3	0.4	0.2	0.2	1
14 and 15		0.05	0.3	0.04	0.2	0.2	1

*Variance matrix $(\delta\sigma/\sigma)$.
[a]For all (n, p) and (n, α) a constant uncertainty value of ±20% has been adopted.
[b]See energy boundary in Table IV.
[c]Read as 4.98×10^{-1}.

established in formal covariance data, and future studies should certainly address these issues to consolidate the results obtained in the present study. In summary, the uncertainty values used in this study are preliminary but allow reasonable and quantitative indications of their impact. In fact, to point out outstanding problems and areas of concern, an exact answer is not the major requirement but rather a physics insight on a very large number of data with different sensitivities.

IV.B. Uncertainty on the Multiplication Factor

The results of the uncertainty analysis for k_{eff} are given in compact form in Tables VII and VIII, obtained with the hypothesis of no correlation in energy among reactions or isotopes, as previously indicated. Table VII is a summary by energy group and reaction type. Each value is the square root of the sum of the squares, for a specific reaction type, of each isotope's contributions. Table VIII gives the summary by isotope and reaction type. Each value is the square root of the sum of the squares, for a specific reaction type, of each energy group value. The total uncertainties quoted in Tables VII and VIII are the square root of the sum of the squares of the values for each single group or isotope, respectively.

The total value ($\pm 2.77\%$) is fairly significant, and it is much higher than corresponding values obtained for standard critical cores. The major contributors among actinides are ^{241}Am, ^{243}Am, ^{244}Cm, ^{237}Np, and ^{239}Pu, and the fission cross-section uncertainties generally play a major role. However, the capture and the inelastic cross-section uncertainties for both ^{241}Am and ^{243}Am have a very significant effect. The case of the inelastic cross section of ^{243}Am is of interest. As shown in Fig. 8, this isotope shows a very large value of σ_{in} in the energy region from 100 keV to 1 MeV, where the neutron flux is high in comparison with other actinides. For that energy region, the spread of evaluations, as given by the major data files, is very significant[23] which justifies the large estimated uncertainty value given in Tables IV, V, and VI.

As for structural materials, ^{56}Fe, Pb, and Bi inelastic cross sections also make a relevant contribution to the total uncertainty on k_{eff}.

The energy breakdown of Table VII indicates that for the fission cross section, for example, the uncertainties in the energy range from 10 keV to ~10 MeV are the most significant. High-energy data are also relevant in the case of the capture cross sections. Both effects are related to the hard neutron spectra found in this type of core, as expected.

As a final remark, these uncertainties, or at least their order of magnitude, would apply to the case of the K_S, defined in Sec. II.B.5, as has been shown in Ref. 9, and would be applicable to a critical version of the subcritical core analyzed here.

IV.C. The Doppler Reactivity Coefficient

As expected, the Doppler reactivity effect is very small, due both to the absence of true fertile isotopes (e.g., ^{238}U) and to the small Doppler effect of isotopes like ^{241}Am in view of their resonance structure. In Fig. 9,

TABLE VII

k_{eff}—Uncertainties by Group—No Energy Correlation*

Group	(MeV)[a]	σ_{cap}	σ_{fiss}	ν	σ_{el}	σ_{inel}	$\sigma_{n,2n}$	Total[b]
1	19.6	0.01	0.05	0.02	—	0.04	0.04	0.08
2	6.07	0.01	0.57	0.18	0.04	0.47	—	0.76
3	2.23	0.03	0.83	0.27	0.07	0.46	—	0.99
4	1.35	0.47	1.56	0.41	0.20	0.77	—	1.86
5	4.98e−1[c]	0.84	0.39	0.08	0.10	0.19	—	0.95
6	1.83e−1	1.01	0.32	0.07	0.06	0.20	—	1.08
7	6.74e−2	0.41	0.24	0.07	0.02	0.04	—	0.49
8	2.48e−2	0.37	0.22	0.04	0.02	0.03	—	0.43
9	9.12e−3	0.31	0.20	0.03	—	—	—	0.37
10	2.04e−3	0.20	0.08	0.02	—	—	—	0.21
11	4.54e−4	0.04	0.01	—	—	—	—	0.04
12	2.26e−5	—	—	—	—	—	—	—
13	4.00e−6	—	—	—	—	—	—	—
14	5.40e−7	—	—	—	—	—	—	—
15	1.00e−7	—	—	—	—	—	—	—
Total[b]		1.54	1.97	0.54	0.25	1.05	0.04	2.77

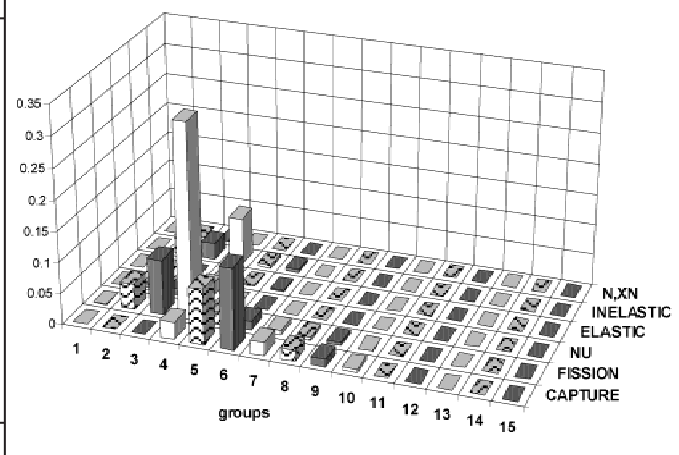

*Uncertainties (%).
[a]High-energy group boundary.
[b]Total obtained as the square root of the sum of the squares of individual contributions in row or column.
[c]Read as 4.98×10^{-1}.

TABLE VIII

k_{eff}—Uncertainties by Isotope—No Energy Correlation*

Isotope	σ_{cap}	σ_{fiss}	ν	σ_{el}	σ_{inel}	$\sigma_{n,2n}$	Total[a]
^{238}Pu	0.01	0.11	0.02	—	—	—	0.11
^{239}Pu	0.04	0.51	0.11	—	0.04	—	0.53
^{240}Pu	0.05	0.18	0.05	—	0.02	—	0.19
^{241}Pu	0.04	0.30	0.03	—	0.01	—	0.31
^{242}Pu	0.01	0.05	0.02	—	0.01	—	0.06
^{237}Np	0.24	0.70	0.21	—	0.14	—	0.78
^{241}Am	1.32	1.12	0.38	—	0.22	—	1.79
^{242m}Am	0.01	0.09	0.03	—	0.01	—	0.10
^{243}Am	0.74	0.59	0.21	—	0.60	—	1.14
^{242}Cm	—	—	—	—	—	—	—
^{243}Cm	—	0.05	0.01	—	—	—	0.05
^{244}Cm	0.13	1.09	0.18	—	0.07	—	1.11
^{245}Cm	0.01	0.41	0.08	—	0.01	—	0.42
^{246}Cm	—	—	—	—		—	—
^{56}Fe	0.03	—	—	0.05	0.49	—	0.50
^{57}Fe	—	—	—	—	0.06	—	0.06
^{52}Cr	0.01	—	—	0.01	0.03	—	0.03
^{58}Ni	—	—	—	—		—	—
Zr	0.03	—	—	0.03	0.07	—	0.09
^{15}N	—	—	—	0.19	0.01	—	0.19
Pb	0.02	—	—	0.10	0.41	0.02	0.43
Bi	0.04	—	—	0.11	0.49	0.03	0.50
Total[a]	1.54	1.97	0.54	0.25	1.05	0.04	2.77

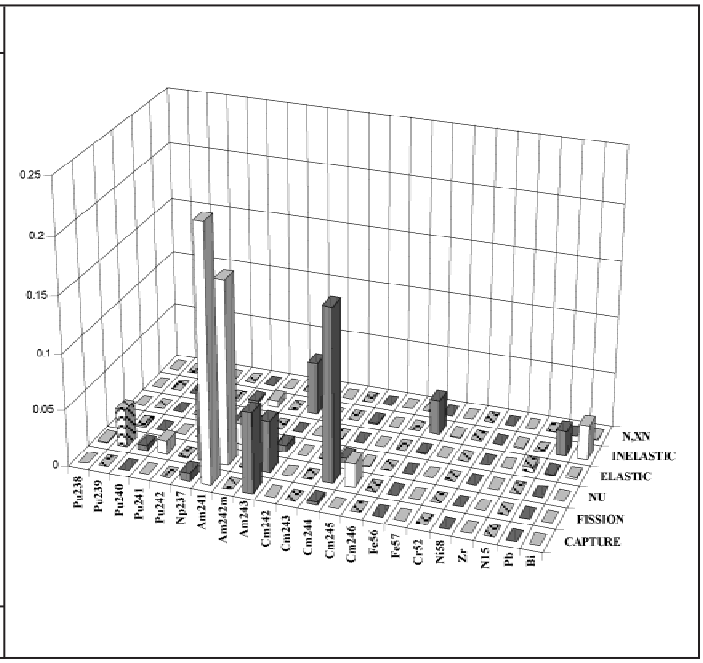

*Uncertainties (%).
[a]Total obtained as the square root of the sum of the squares of individual contributions in row or column.

the capture cross sections below 10 keV of ^{241}Am are compared to those of ^{238}U, ^{239}Pu, and ^{241}Pu. Very little resonance structure is observed above 100 eV.

The resonance structure of ^{241}Am is such that self-shielding effects and, consequently, the Doppler effect on the self-shielding in a hard neutron spectrum, as the one found in MA transmuter systems, are much smaller than for other fissile and fertile isotopes. To show this feature quantitatively, we have calculated self-shielding factors corresponding to different potential cross sections (σ_p = 5, 100, and 500 b), and in the case of σ_p = 100 b, at two different temperatures (see Table IX).

As an example, at σ_p = 100 b and at energy between ~1 keV and 200 eV, the self shielding effect $(1 - f)$ on the capture cross section increases for a temperature increase from 300 to 980 K by ~20% in the case of ^{239}Pu, by ~30% in the case of ^{238}U, and by <5% in the case of ^{241}Am. In this situation, a sensitivity/uncertainty analysis as outlined in Sec. II.B for indirect effects is fairly irrelevant, the most important uncertainty being associated

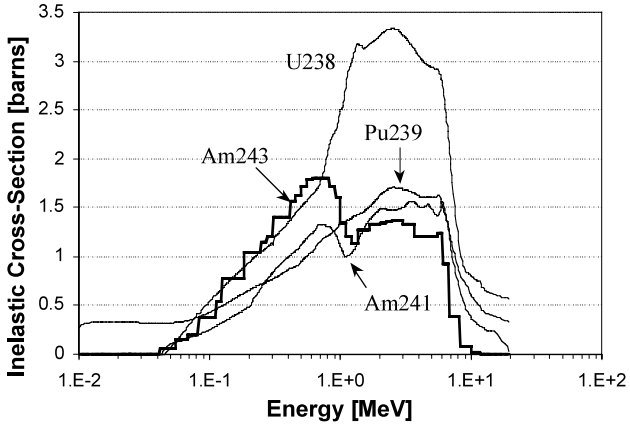

Fig. 8. Inelastic cross section for selected actinides.

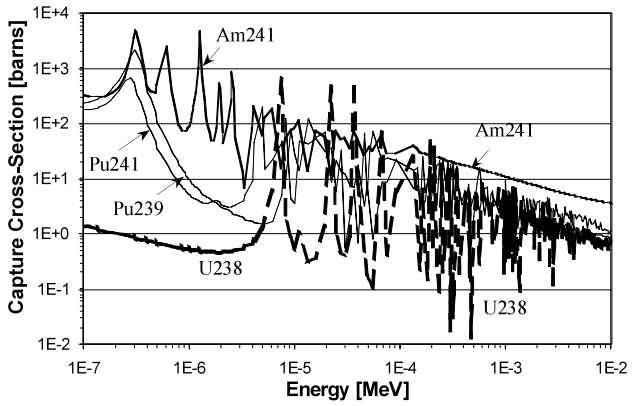

Fig. 9. Capture (n, γ) cross section for selected actinides.

TABLE IX

Self-Shielding Factor for the Capture Cross Sections of ^{239}Pu, ^{241}Pu, ^{241}Am, and ^{238}U

Isotope	^{239}Pu				^{241}Pu				^{241}Am				^{238}U			
σ_p (b)	5	100		500	5	100		500	5	100		500	5	100		500
T (K)	300	300	980	300	300	300	980	300	300	300	980	300	300	300	980	300
Energy (MeV)	f	f	f	f	f	f	f	f	f	f	f	f	f	f	f	f
9.12E−03[a]	0.89	0.92	0.95	0.99	0.91	0.95	0.96	1.00	0.95	0.98	0.98	1.00	0.89	0.84	0.90	0.98
5.53E−03	0.88	0.90	0.93	0.99	0.88	0.92	0.95	0.99	0.92	0.96	0.97	1.00	0.83	0.77	0.86	0.97
3.35E−03	0.77	0.86	0.91	0.99	0.85	0.89	0.92	0.99	0.91	0.94	0.96	1.00	0.81	0.76	0.86	0.95
2.03E−03	0.82	0.90	0.98	0.99	0.82	0.85	0.89	0.98	0.88	0.90	0.92	0.99	0.65	0.58	0.68	0.90
1.23E−03	0.70	0.81	0.93	0.97	0.77	0.84	0.89	0.98	0.93	0.91	0.93	0.99	0.53	0.47	0.58	0.85
7.49E−04	0.51	0.66	0.77	0.94	0.63	0.71	0.78	0.96	0.89	0.86	0.89	0.98	0.46	0.38	0.49	0.82
4.54E−04	0.42	0.55	0.67	0.92	0.60	0.67	0.79	0.94	0.80	0.83	0.88	0.97	0.41	0.34	0.43	0.75
3.04E−04	0.26	0.44	0.57	0.85	0.13	0.65	0.70	0.92	0.67	0.74	0.84	0.95	0.24	0.19	0.24	0.59
1.49E−04	0.22	0.37	0.46	0.83	0.34	0.60	0.66	0.93	0.34	0.59	0.68	0.92	0.16	0.12	0.14	0.43
9.17E−05	0.11	0.18	0.21	0.64	0.21	0.42	0.48	0.89	0.37	0.59	0.69	0.94	0.42	0.32	0.42	0.83
6.79E−05	0.06	0.15	0.16	0.64	0.37	0.52	0.51	0.94	0.31	0.51	0.59	0.91	0.13	0.10	0.11	0.39
4.02E−05	0.30	0.38	0.44	0.80	0.37	0.42	0.44	0.89	0.29	0.42	0.49	0.88	0.11	0.10	0.10	0.30
2.26E−05	0.13	0.16	0.18	0.59	0.12	0.17	0.19	0.56	0.17	0.23	0.26	0.66	0.11	0.10	0.11	0.31
1.37E−05	0.14	0.22	0.23	0.63	0.13	0.19	0.21	0.61	0.23	0.32	0.36	0.80	1.06	1.09	1.10	1.01
8.32E−06	0.09	0.13	0.13	0.48	0.33	0.43	0.16	0.50	0.15	0.23	0.25	0.64	0.15	0.15	0.16	0.35
4.00E−06	0.22	0.22	0.22	0.69	0.47	0.22	0.25	0.81	0.07	0.10	0.11	0.40	1.00	1.00	1.00	1.00

[a]Read as 9.12×10^{-3}.

with direct effects, i.e., to the self-shielding factors themselves. Table X shows the actual self-shielding factor for the ^{241}Am capture cross section in the system under study. The corresponding potential cross section σ_p has been evaluated to ~400 b. A detailed resonance data reassessment for isotopes like ^{241}Am seems then appropriate to improve the confidence in the Doppler calculation of a core with a MA-dominated fuel.

TABLE X

Self-Shielding Factors for the Capture Cross Section of ^{241}Am in the System Under Study

Energy (MeV)	f	Energy (MeV)	f
9.12E−03[a]	1.00	9.17E−05	0.96
5.53E−03	1.00	6.79E−05	0.90
3.35E−03	1.00	4.02E−05	0.93
2.03E−03	1.00	2.26E−05	0.86
1.23E−03	1.00	1.37E−05	0.92
7.49E−04	0.99	8.32E−06	0.59
4.54E−04	1.00	4.00E−06	0.41
3.04E−04	1.00	5.40E−06	0.86
1.49E−04	0.94	1.00E−06	0.99

[a]Read as 9.12×10^{-3}.

IV.D. The Coolant Void Reactivity Effect

A perturbation component breakdown of the coolant void reactivity coefficient, both by energy group and by isotope (see Tables XI and XII), reveals the peculiar nature of that coefficient in the system considered. The positive spectral component (sum of the elastic + inelastic + (n, xn) removal) is higher than the leakage effect. That high value is directly related to the shape of the adjoint flux discussed previously (see Sec. III.B and Fig. 6). The compensation of positive and negative contributions to the spectral effect, which can be written in perturbation terms as

$$\Delta\rho^{Spec} \div \frac{n^{cool}}{\langle \underline{\Phi}^*, F\underline{\Phi} \rangle} \int \sigma_{scat}^{cool}(E \to E')\underline{\Phi}(E,r) \times [\underline{\phi}^*(E',r) - \underline{\Phi}^*(E,r)]\, dE\, dE'\, dr \ , \qquad (37)$$

where n^{cool} and σ_{scatt}^{cool} are, respectively, the number density and the total scattering cross section of the coolant, is due to the energy shape of the adjoint flux $\underline{\Phi}^*$. In fact, inspection of Fig. 6 allows us to understand the high positive value of the spectral component in the system under consideration.

The sensitivity analysis and the results of the uncertainty analysis underline the major role played by the

TABLE XI

Energy Group Breakdown of the Core Coolant Void Reactivity by Component*

Group	Energy (MeV)	Capture	Fission	Leakage	Elastic Removal	Inelastic + (n, xn) Removal	Sum
1	1.964E+1[a]	0.4	−0.4	−11.2	2.8	−31.3	−39.8
2	1.000E+1	0.5	—	−58.3	7.4	203.8	153.4
3	6.065E+0	4.4	0.5	−221.9	−18.2	842.5	607.3
4	3.679E+0	20.9	5.8	−483.2	61.4	1413.5	1018.4
5	2.231E+0	45.1	12.8	−786.1	252.3	1487.0	1011.0
6	1.353E+0	53.1	40.8	−695.3	469.6	788.5	656.8
7	8.209E−1	67.3	31.7	−579.9	463.7	70.2	53.0
8	4.979E−1	59.4	−3.1	−401.6	245.0	0.5	−99.9
9	3.020E−1	59.9	0.2	−387.0	114.4	−1.5	−214.1
10	1.832E−1	64.8	−0.3	−296.4	165.2	−0.1	−66.8
11	1.111E−1	49.8	1.0	−189.2	104.8	0.5	−33.2
12	6.738E−2	76.6	0.2	−117.2	60.2	0.2	20.0
13	4.087E−2	41.5	1.4	−62.4	21.5	—	2.1
14	2.479E−2	27.0	1.4	−35.9	12.5	—	4.9
15	1.503E−2	21.6	−3.8	−39.0	9.0	—	−12.1
16	9.119E−3	5.7	−0.4	−5.3	0.3	—	0.4
17	5.531E−3	18.8	−1.0	−4.7	−2.4	—	10.7
18	3.355E−3	31.7	−3.2	0.7	7.1	—	36.3
19	2.035E−3	6.2	−0.3	4.9	1.1	—	11.8
20	1.234E−3	60.6	−3.6	5.3	−9.6	—	52.7
21	7.485E−4	2.4	−1.7	4.3	0.3	—	5.4
22	4.540E−4	0.4	−0.5	1.8	−0.5	—	1.2
23	3.043E−4	1.3	−1.4	3.9	0.1	—	3.9
24	1.486E−4	0.9	−0.4	1.6	−0.2	—	1.9
25	9.166E−5	0.5	−0.7	1.2	0.2	—	1.1
26	6.790E−5	0.9	−0.7	1.3	0.1	—	1.7
27	4.017E−5	0.5	−0.2	0.4	−0.1	—	0.6
28	2.260E−5	0.3	−0.4	0.5	—	—	0.4
29	1.371E−5	0.2	−0.1	0.3	—	—	0.4
30	8.315E−6	0.2	—	0.2	—	—	0.4
31	4.000E−6	—	—	—	—	—	—
32	5.400E−7	—	—	—	—	—	—
33	1.000E−7	—	—	—	—	—	—
Sum		722.7	73.8	−4348.2	1968.0	4773.7	3190.0

*Values are in pcm.
[a]Read as 1.964×10^1.

coolant materials' (i.e., Pb and Bi) inelastic cross-section uncertainties (see Tables XIII through XVI). Note that direct effects on fissile isotopes are coming through their contribution to the normalization integral of the denominator of Eq. (37).

The uncertainty on the leakage term of the void coefficient is related to σ_{el} uncertainties. Since these uncertainties are smaller than σ_{in} uncertainties, the overall uncertainty is determined by the spectral component related data. As for direct versus indirect effect, Tables XIII through XVI show the relevance of direct effects (total value of the related uncertainty: ±24.6%) with respect to indirect effects (±14.2%). As indirect effects (i.e., effects due to the change in shape of the real and the adjoint fluxes), besides Pb and Bi, ^{241}Am, ^{243}Am, and ^{244}Cm play a significant role. Finally, to obtain the total uncertainty value, direct and indirect effects should be summed up (i.e., total uncertainty: ±38.8%).

IV.E. The Effective Delayed-Neutron Fraction

The relatively low nominal value of $\hat{\beta}_{eff}$ for the system under consideration (see Table II) is expected because the delayed-neutron parameters of the MAs (in particular Am and Cm) are smaller than the corresponding parameters for U and Pu isotopes.

TABLE XII

Isotope Breakdown of the Core Coolant Void Reactivity by Component*

	Capture	Fission	Leakage	Elastic Removal	Inelastic + (n, xn) Removal	Sum
^{237}Np	0.3	10.1	—	0.1	0.9	11.3
^{238}Pu	—	1.1	—	—	—	1.1
^{239}Pu	3.8	−9.2	0.1	—	0.5	−4.8
^{240}Pu	1.2	6.5	—	0.1	0.7	8.5
^{241}Pu	0.2	0.7	—	—	—	0.9
^{242}Pu	0.2	2.1	—	—	—	2.5
^{241}Am	4.3	34.9	0.1	—	1.4	40.7
^{242m}Am	—	0.4	—	—	—	0.4
^{243}Am	3.1	17.9	−0.1	0.4	−3.7	17.6
^{242}Cm	—	—	—	—	—	—
^{243}Cm	—	0.1	—	—	—	0.1
^{244}Cm	2.6	8.9	—	0.2	0.3	11.9
^{245}Cm	—	0.4	—	—	0.1	0.5
Zr	23.8	—	−6.6	36.2	−16.3	37
^{15}N	—	—	−7.5	132.7	—	125.2
Fe	61	—	−79.1	121.3	4.6	107.9
Cr	3.9	—	−5.8	15.5	−5.7	7.9
Ni	−0.3	—	0.1	0.4	−0.2	—
Mo	—	—	—	0.3	−0.2	—
Mn	0.8	—	—	0.8	0.3	1.9
W	0.3	—	—	—	—	0.3
Pb	224.2	—	−1913.2	728.3	2229.5	1268.8
Bi	393.2	—	−2336.3	929.2	2561.4	1547.5
Sum	722.7	73.8	−4348.3	1965.5	4773.7	3187.4

*Values are in pcm.

TABLE XIII

Void Coefficient—Uncertainties by Group—Direct Effect*

Group	(MeV)[a]	σ_{cap}	σ_{fiss}	ν	σ_{el}	σ_{inel}	$\sigma_{n,2n}$	Total[b]
1	19.6	—	0.1	—	—	1.8	1.7	2.5
2	6.07	0.1	1.1	0.2	1.9	18.7	—	18.9
3	2.23	0.2	1.3	0.3	2.3	12.6	—	12.8
4	1.35	0.5	1.9	0.3	2.3	8.0	—	8.6
5	4.98E−1[c]	0.5	0.5	0.1	1.8	0.1	—	1.9
6	1.83E−1	0.4	0.4	0.1	1.0	—	—	1.1
7	6.74E−2	0.6	0.3	0.1	0.4	—	—	0.7
8	2.48E−2	0.2	0.2	—	0.3	—	—	0.4
9	9.12E−3	0.2	0.2	—	—	—	—	0.3
10	2.04E−3	0.3	0.1	—	—	—	—	0.3
11	4.54E−4	—	—	—	—	—	—	—
12	2.26E−5	—	—	—	—	—	—	—
13	4.00E−6	—	—	—	—	—	—	—
14	5.40E−7	—	—	—	—	—	—	—
15	1.00E−7	—	—	—	—	—	—	—
Total[b]		1.1	2.7	0.5	4.3	24.0	1.7	24.6

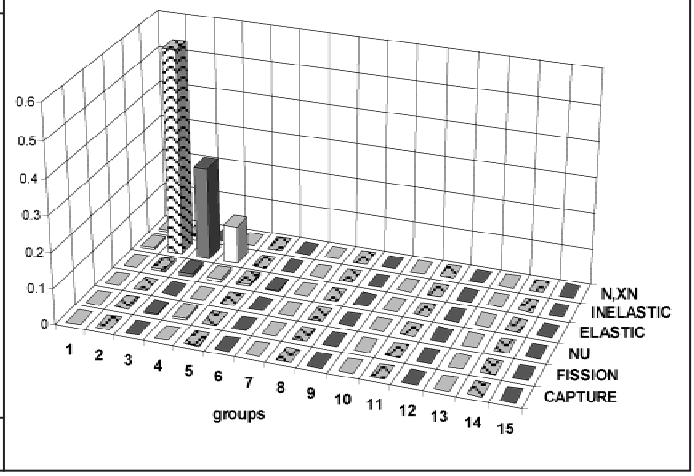

*Uncertainties (%).
[a]High-energy group boundary.
[b]Total obtained as the square root of the sum of the squares of individual contributions in row or column.
[c]Read as 4.98×10^{-1}.

TABLE XIV

Void Coefficient—Uncertainties by Isotope—Direct Effect*

Isotope	σ_{cap}	σ_{fiss}	ν	σ_{el}	σ_{inel}	$\sigma_{n,2n}$	Total[a]
^{238}Pu	—	0.1	—	—	—	—	0.1
^{239}Pu	—	0.6	0.1	—	—	—	0.7
^{240}Pu	—	0.2	—	—	—	—	0.3
^{241}Pu	—	0.4	—	—	—	—	0.4
^{242}Pu	—	0.1	—	—	—	—	0.1
^{237}Np	—	1.0	0.2	—	—	—	1.0
^{241}Am	0.1	1.6	0.4	—	—	—	1.6
^{242m}Am	—	0.1	—	—	—	—	0.1
^{243}Am	—	0.9	0.2	—	0.1	—	0.9
^{242}Cm	—	—	—	—	—	—	—
^{243}Cm	—	0.1	—	—	—	—	0.1
^{244}Cm	—	1.4	0.2	—	—	—	1.5
^{245}Cm	—	0.5	0.1	—	—	—	0.5
^{246}Cm	—	—	—	—	—	—	—
^{56}Fe	0.1	—	—	0.1	0.1	—	0.2
^{57}Fe	—	—	—	—	—	—	—
^{52}Cr	—	—	—	—	—	—	—
^{58}Ni	—	—	—	—	—	—	—
Zr	—	—	—	0.1	—	—	0.1
^{15}N	—	—	—	0.2	—	—	0.2
Pb	0.6	—	—	2.8	14.9	0.9	15.2
Bi	0.9	—	—	3.2	18.8	1.5	19.2
Total[a]	1.1	2.7	0.5	4.3	24.0	1.7	24.6

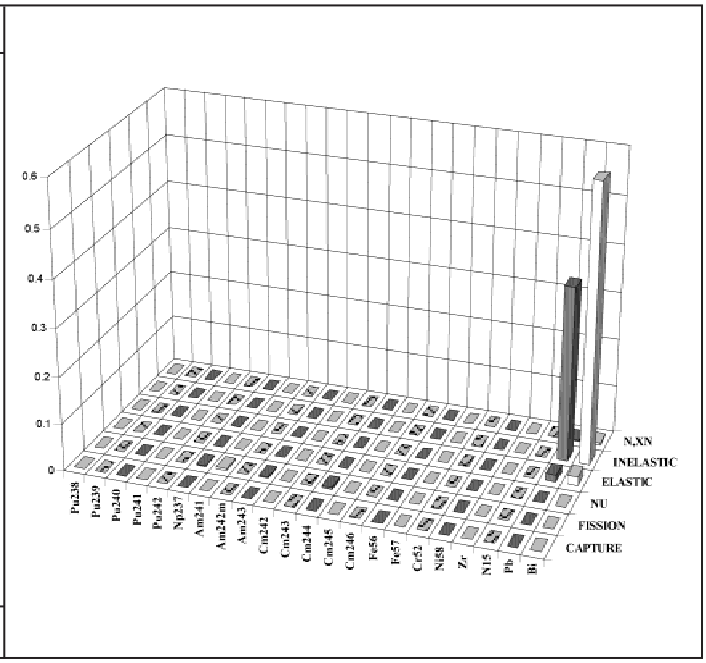

*Uncertainties (%).
[a]Total obtained as the square root of the sum of the squares of individual contributions in row or column.

The uncertainty analysis related to indirect effects, performed on the basis of the formulations of Sec. II.B.7, is summarized in Tables XVII and XVIII.

The overall uncertainty due to indirect effects is ±10%, with a relevant contribution of ^{241}Am, ^{243}Am, and ^{244}Cm data and some impact of the coolant material

TABLE XV

Void Coefficient—Uncertainties by Group—Indirect Effect*

Group	(MeV)[a]	σ_{cap}	σ_{fiss}	ν	σ_{el}	σ_{inel}	$\sigma_{n,2n}$	Total[b]
1	19.6	0.1	0.7	0.2	0.1	0.9	0.9	1.5
2	6.07	0.1	4.9	1.7	1.9	9.2	—	10.7
3	2.23	0.1	1.6	0.6	2.2	2.5	—	3.7
4	1.35	0.9	2.2	0.5	2.9	1.3	—	4.0
5	4.98E−1[c]	2.8	1.0	0.2	2.1	1.1	—	3.8
6	1.83E−1	3.8	1.0	0.2	1.6	0.5	—	4.3
7	6.74E−2	2.2	1.2	0.4	0.3	0.3	—	2.6
8	2.48E−2	2.1	1.2	0.2	0.2	0.4	—	2.5
9	9.12E−3	2.2	1.5	0.2	0.1	—	—	2.6
10	2.04E−3	1.0	0.5	0.1	0.1	—	—	1.1
11	4.54E−4	0.1	—	—	0.1	—	—	0.1
12	2.26E−5	—	—	—	—	—	—	—
13	4.00E−6	—	—	—	—	—	—	—
14	5.40E−7	—	—	—	—	—	—	—
15	1.00E−7	—	—	—	—	—	—	—
Total[b]		6.2	6.2	1.9	4.9	9.7	0.9	14.2

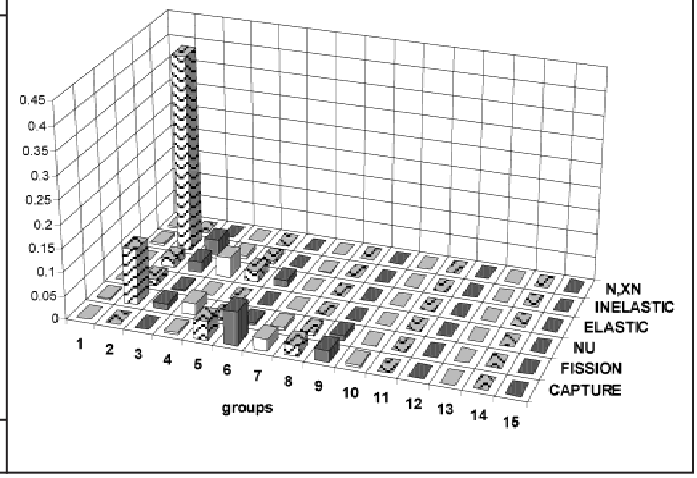

*Uncertainties (%).
[a]High-energy group boundary.
[b]Total obtained as the square root of the sum of the squares of individual contributions in row or column.
[c]Read as 4.98×10^{-1}.

TABLE XVI

Void Coefficient—Uncertainties by Isotope—Indirect Effect*

Isotope	σ_{cap}	σ_{fiss}	ν	σ_{el}	σ_{inel}	$\sigma_{n,2n}$	Total[a]
^{238}Pu	—	0.3	0.1	—	—	—	0.3
^{239}Pu	0.2	1.7	0.5	—	0.2	—	1.8
^{240}Pu	0.2	0.4	0.1	—	0.1	—	0.5
^{241}Pu	0.1	1.3	0.1	—	0.1	—	1.3
^{242}Pu	0.1	0.1	—	—	0.1	—	0.1
^{237}Np	1.2	1.8	0.6	—	0.8	—	2.4
^{241}Am	5.2	3.9	1.5	—	1.2	—	6.8
^{242m}Am	—	0.4	0.1	—	—	—	0.4
^{243}Am	3.1	2.1	0.8	—	2.0	—	4.3
^{242}Cm	—	—	—	—	—	—	—
^{243}Cm	—	0.2	—	—	—	—	0.2
^{244}Cm	0.6	2.8	0.5	—	0.4	—	3.0
^{245}Cm	—	1.7	0.3	—	—	—	1.7
^{246}Cm	—	—	—	—	—	—	—
^{56}Fe	0.1	—	—	1.7	1.8	—	2.5
^{57}Fe	—	—	—	0.1	0.5	—	0.5
^{52}Cr	—	—	—	0.5	0.2	—	0.6
^{58}Ni	—	—	—	—	—	—	—
Zr	0.1	—	—	0.6	1.3	—	1.4
^{15}N	—	—	—	0.6	0.1	—	0.6
Pb	0.1	—	—	2.9	5.2	0.5	6.0
Bi	0.1	—	—	3.4	7.5	0.7	8.3
Total[a]	6.2	6.2	1.9	4.9	9.7	0.9	14.2

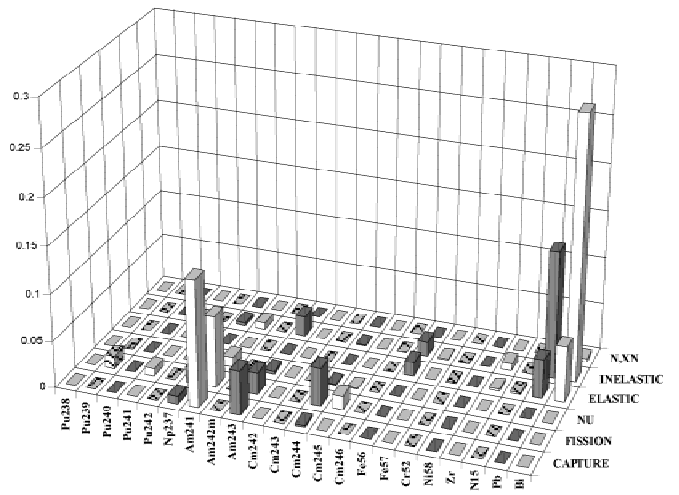

*Uncertainties (%).
[a]Total obtained as the square root of the sum of the squares of individual contributions in row or column.

TABLE XVII

$\hat{\beta}_{eff}$—Uncertainties by Group—Indirect Effect*

Group	(MeV)[a]	σ_{cap}	σ_{fiss}	ν	σ_{el}	σ_{inel}	$\sigma_{n,2n}$	Total[b]
1	19.6	—	0.3	0.1	—	0.2	0.2	0.5
2	6.07	0.1	3.1	1.0	0.3	2.8	—	4.3
3	2.23	0.2	4.0	1.3	0.4	2.4	—	4.9
4	1.35	0.6	3.1	0.9	0.3	2.1	—	3.8
5	4.98E−1[c]	2.2	0.9	0.2	0.3	0.6	—	2.5
6	1.83E−1	4.4	1.3	0.3	0.3	0.8	—	4.6
7	6.74E−2	2.1	1.1	0.3	0.2	0.1	—	2.4
8	2.48E−2	1.9	1.1	0.2	0.2	0.1	—	2.2
9	9.12E−3	1.5	0.9	0.2	—	—	—	1.8
10	2.04E−3	0.8	0.3	0.1	—	—	—	0.9
11	4.54E−4	0.1	0.1	—	—	—	—	0.1
12	2.26E−5	—	—	—	—	—	—	—
13	4.00E−6	—	—	—	—	—	—	—
14	5.40E−7	—	—	—	—	—	—	—
15	1.00E−7	—	—	—	—	—	—	—
Total[b]		5.9	6.4	2.0	0.8	4.4	0.2	10.0

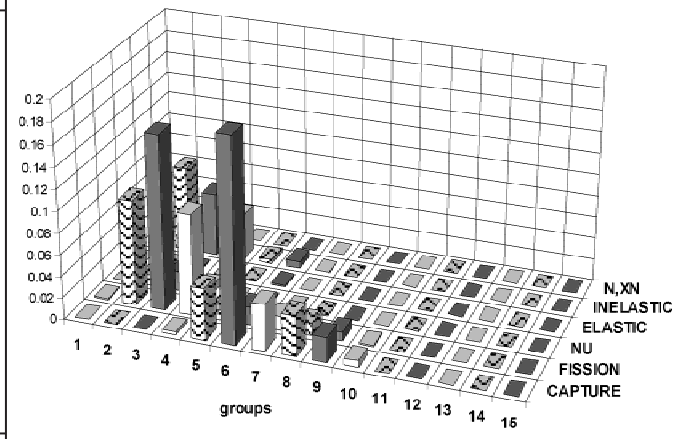

*Uncertainties (%).
[a]High-energy group boundary.
[b]Total obtained as the square root of the sum of the squares of individual contributions in row or column.
[c]Read as 4.98×10^{-1}.

TABLE XVIII

$\hat{\beta}_{eff}$—Uncertainties by Isotope—Indirect Effect*

Isotope	σ_{cap}	σ_{fiss}	ν	σ_{el}	σ_{inel}	$\sigma_{n,2n}$	Total[a]
^{238}Pu	—	0.3	0.1	—	—	—	0.3
^{239}Pu	0.2	1.5	0.4	—	0.1	—	1.5
^{240}Pu	0.2	0.5	0.1	—	0.1	—	0.5
^{241}Pu	0.1	1.3	0.1	—	—	—	1.3
^{242}Pu	0.1	0.1	—	—	—	—	0.2
^{237}Np	1.1	1.9	0.6	—	0.6	—	2.3
^{241}Am	5.0	4.2	1.5	—	0.8	—	6.7
^{242m}Am	—	0.3	0.1	—	—	—	0.4
^{243}Am	2.9	2.3	0.8	—	1.9	—	4.3
^{242}Cm	—	—	—	—	—	—	—
^{243}Cm	—	0.2	—	—	—	—	0.2
^{244}Cm	0.6	2.9	0.5	—	0.3	—	3.0
^{245}Cm	—	1.6	0.3	—	—	—	1.6
^{246}Cm	—	—	—	—	—	—	—
^{56}Fe	0.1	—	—	0.1	1.6	—	1.6
^{57}Fe	—	—	—	—	0.1	—	0.1
^{52}Cr	—	—	—	—	0.1	—	0.1
^{58}Ni	—	—	—	—	—	—	—
Zr	0.1	—	—	0.1	0.4	—	0.5
^{15}N	—	—	—	0.4	—	—	0.4
Pb	0.1	—	—	0.4	2.0	0.1	2.1
Bi	0.2	—	—	0.5	2.7	0.2	2.8
Total[a]	5.9	6.4	2.0	0.8	4.4	0.2	10.0

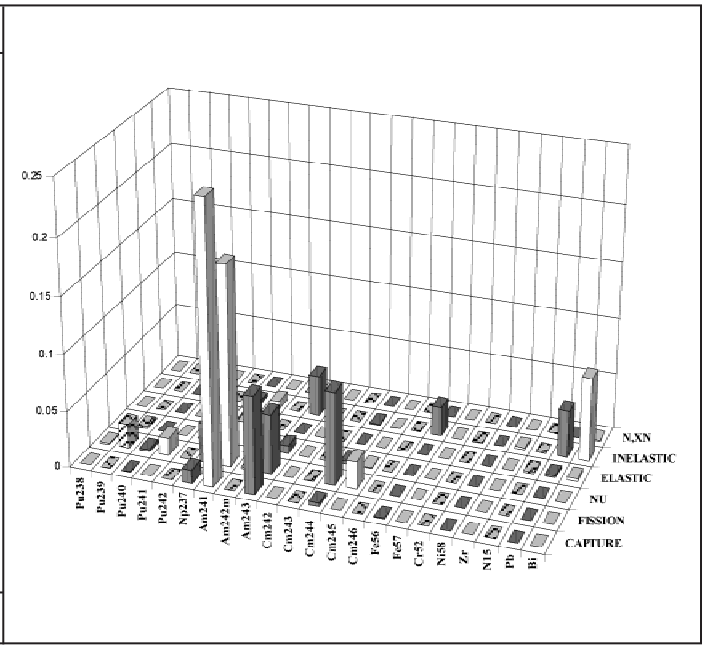

*Uncertainties (%).

[a]Total obtained as the square root of the sum of the squares of individual contributions in row or column.

cross sections (Pb and Bi). As for direct effects, the major contribution comes from the uncertainty on the mean values of the delayed-neutron yields.[24] The sensitivity coefficients are given by (for each fissile isotope m)

$$S(\nu_m^d) = \frac{\hat{\beta}_{eff}^m}{\hat{\beta}_{eff}} \quad . \tag{38}$$

The value of these sensitivity coefficients is given in Table XIX. The uncertainties to be used with these coefficients can be deduced by the extensive work documented in Ref. 25. Accounting for the existing measurements and their associated experimental uncertainties, a value of ±10% can be associated with Pu isotopes and ±20% with MAs. This gives a value of uncertainty of ±5.3% on $\hat{\beta}_{eff}$ due to the direct effect which can be combined to the indirect effect to give a total uncertainty of approximately ±15%. Note that a further uncertainty should also be associated with the spectra of the delayed neutrons. But this will modify only slightly the value quoted previously, since the sensitivity of $\hat{\beta}_{eff}$ to variations of the χ_i^d is relatively small.[24]

IV.F. The Reactivity Loss During Irradiation

This parameter plays an important role in the overall performance assessment of a dedicated core because the dominating MA isotopes in the fresh fuel are transformed during irradiation in more reactive isotopes (as in the transmutation of ^{241}Am into ^{242}Am, ^{237}Np into ^{238}Pu, ^{244}Cm into ^{245}Cm, etc.). This fact could give rise to a reactivity increase during irradiation, and the introduction of Pu in the fresh fuel is a measure to counterbalance that effect because the burnup of ^{239}Pu and ^{241}Pu results in a strong reactivity loss. Inspection of Table XX, which gives the perturbation breakdown of the total effect,

TABLE XIX

Direct Effect Sensitivity Coefficients (%) for $\hat{\beta}_{eff}$*

	^{237}Np	^{238}Pu	^{239}Pu	^{240}Pu	^{241}Pu	^{242}Pu	^{241}Am	^{242m}Am	^{243}Am	^{243}Cm	^{244}Cm	^{245}Cm
$\hat{\beta}_{eff}^m/\hat{\beta}_{eff}$	12.07	1.32	33.01	5.34	25.87	3.30	5.83	1.10	7.32	0.13	2.46	2.24

*Values are in percent.

TABLE XX

$\Delta\rho^{cycle}$ (1 yr)—Perturbation Breakdown by Isotope*

Isotope	Capture	Fission	Elastic Removal	Inelastic + (n, xn) Removal	Sum
^{234}U	−2.5	6.0	—	−0.9	2.6
^{235}U	−0.1	1.2	—	0	1.1
^{236}U	−0.1	0.1	—	0	−0.1
^{237}Np	616.6	−659.9	−1.7	74.8	29.8
^{238}Pu	−264.5	3060.5	—	−55.4	2740.6
^{239}Pu	277.2	−5389.0	−2.2	82.2	−5031.8
^{240}Pu	−28.6	108.6	0.8	−7.5	73.3
^{241}Pu	100.9	−2032.1	−0.9	19	−1913.2
^{242}Pu	−43.2	139.5	0.6	−11.6	85.2
^{241}Am	1712.8	−1620.4	−2.6	127.3	217.0
^{242m}Am	−39.3	1354.4	−0.2	−21	1293.9
^{242f}Am	−1.1	29.3	—	−0.3	28.0
^{243}Am	870.9	−700.3	−0.9	199.1	368.8
^{242}Cm	−119.2	986.2	−0.1	−45.1	821.9
^{243}Cm	−0.1	14.1	—	−0.1	13.9
^{244}Cm	−135.6	735.6	−0.2	−36.6	563.1
^{245}Cm	−5.6	327.0	0.1	−2.4	319.1
^{246}Cm	−1.2	10.8	—	−0.7	8.8
^{247}Cm	—	1.3	—	0	1.3
Fission products	−574	0	−41.1	−286.3	−901.3
Sum	2363.2	−3627.3	−48.6	34.6	−1278.2

*Values in pcm.

allows us to see clearly the different effects and their order of magnitude. The total $\Delta\rho^{cycle}$ value is then the result of the compensation of large positive and negative contributions. This situation can give rise to large direct effects [both due to δn^K and $\Delta\rho^K$, see Eq. (22) in Sec. II.B.4], and indirect effects will play a lesser role. This is confirmed by the results of the uncertainty analysis summarized in Tables XXI through XXIV. The total uncertainty value is large, as expected ($\approx\pm 50\%$, $\sim$600 pcm) and can have significant effects. For example, in the case of an ADS and for a compensation of the reactivity loss by a change of the proton beam current, one should allow a relevant margin on the maximum current required from the accelerator to allow for uncertainties on the nominal value of $\Delta\rho^{cycle}$.

As expected, ^{241}Am, ^{243}Am, ^{242m}Am, and ^{244}Cm capture and fission data uncertainties play a major role.

As anticipated in Sec. II.B.3, in this analysis we neglected the coupling between the nuclide density variation and flux field because it is assumed to be of negligible impact. In fact, Fig. 10 shows the comparison of the flux spectrum calculated at beginning of life (BOL) and at end of life (EOL). The difference is practically insignificant, which is confirmed by inspection of one-group cross sections calculated at BOL and at EOL (see Table XXV).

Finally, sensitivity coefficients for nuclide density variation obtained with the cross sections determined at BOL do not change significantly if calculated at EOL. Even the average flux level in the core changes just from 1.944×10^{15} n/s·cm^{-2} at BOL to 2.018×10^{15} n/s·cm^{-2} at EOL.

IV.G. The Decay Heat

The value quoted in Table II was obtained using the data of the ORIGEN code.[19] The breakdown of the contribution of heavy isotopes, fission products, and light isotopes is given in Table XXVI. The contribution of separated heavy isotopes is given in Table XXVII. As far as the relative contributions of heavy elements, light elements, and fission product and their evolution in time, a comparison (see Table XXVIII) with the values obtained for the typical fast reactor SUPERPHENIX (Ref. 26) indicates that the presence of MAs in the fuel increases the contribution of heavy isotopes with respect to the fission product component already at short cooling times, in particular due to the presence of Cm.

We have not attempted a full uncertainty analysis of the decay heat data, such as the one documented in Ref. 27. However, partial but significant information can be obtained using the uncertainties on the nuclide

TABLE XXI

$\Delta\rho^{cycle}$ (1 yr)—Uncertainties by Isotope—Indirect Effect*

Isotope	σ_{cap}	σ_{fiss}	ν	σ_{el}	σ_{inel}	$\sigma_{n,2n}$	Total[a]
^{238}Pu	0.03	0.24	0.04	—	0.01	—	0.24
^{239}Pu	0.21	1.47	0.37	—	0.10	—	1.53
^{240}Pu	0.16	0.19	0.05	—	0.06	—	0.26
^{241}Pu	0.09	1.16	0.10	—	0.03	—	1.16
^{242}Pu	0.06	0.04	0.02	—	0.03	—	0.08
^{237}Np	1.22	0.48	0.21	—	0.47	—	1.41
^{241}Am	3.56	1.06	0.50	—	0.68	—	3.81
^{242m}Am	0.02	0.37	0.11	—	0.02	—	0.39
^{243}Am	2.36	0.55	0.28	—	0.95	—	2.62
^{242}Cm	—	—	—	—	—	—	—
^{243}Cm	—	0.18	0.03	—	—	—	0.18
^{244}Cm	0.58	0.85	0.19	—	0.27	—	1.08
^{245}Cm	0.05	1.67	0.32	—	0.03	—	1.70
^{246}Cm	—	—	—	—	—	—	—
^{56}Fe	0.12	—	—	0.17	1.24	—	1.26
^{57}Fe	0.02	—	—	0.01	0.18	—	0.18
^{52}Cr	0.03	—	—	0.06	0.13	—	0.14
^{58}Ni	—	—	—	—	0.01	—	0.01
Zr	0.10	—	—	0.09	0.41	—	0.43
^{15}N	0.01	—	—	0.43	0.05	—	0.43
Pb	0.05	—	—	0.29	2.13	0.03	2.15
Bi	0.15	—	—	0.36	2.84	0.06	2.86
Total[a]	4.50	2.99	0.82	0.66	4.00	0.06	6.80

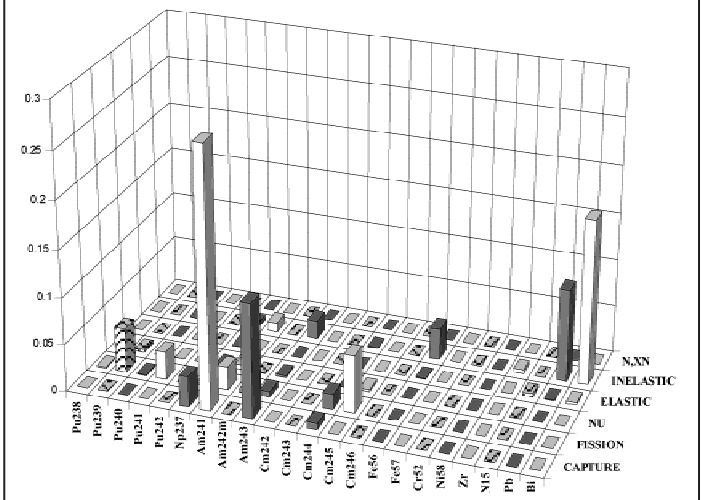

*Uncertainties (%).
[a]Total obtained as the square root of the sum of the squares of individual contributions in row or column.

densities at EOL, which is discussed in Sec. IV.H. A substantial improvement of decay-heat-related data is needed in the case of MA-dominated fuel if a decay heat target accuracy of ±10% is required for future design studies, in particular at long decay times as for repository impact evaluation.

To better quantify needs, a separate detailed analysis is required.

TABLE XXII

$\Delta\rho^{cycle}$ (1 yr)—Uncertainties by Group—Direct Effect of $\delta\sigma$*

Group	(MeV)[a]	σ_{cap}	σ_{fiss}	ν	σ_{el}	σ_{inel}	$\sigma_{n,2n}$	Total[b]
1	19.6	—	0.6	0.2	—	0.1	—	0.6
2	6.07	0.1	6.4	1.9	—	1.6	—	6.9
3	2.23	0.3	9.5	2.9	—	2.7	—	10.3
4	1.35	5.3	20.9	5.1	—	5.6	—	22.9
5	4.98E−1[c]	9.7	12.0	2.4	—	1.9	—	15.7
6	1.83E−1	11.8	7.7	1.7	—	2.0	—	14.3
7	6.74E−2	4.9	5.5	1.4	—	0.2	—	7.5
8	2.48E−2	4.5	4.7	1.0	—	—	—	6.6
9	9.12E−3	3.9	4.0	0.9	—	—	—	5.7
10	2.04E−3	2.5	1.9	0.5	—	—	—	3.2
11	4.54E−4	0.4	0.3	0.1	—	—	—	0.5
12	2.26E−5	—	—	—	—	—	—	—
13	4.00E−6	—	—	—	—	—	—	—
14	5.40E−7	—	—	—	—	—	—	—
15	1.00E−7	—	—	—	—	—	—	—
Total[b]		18.1	29.0	7.2	—	7.0	—	35.6

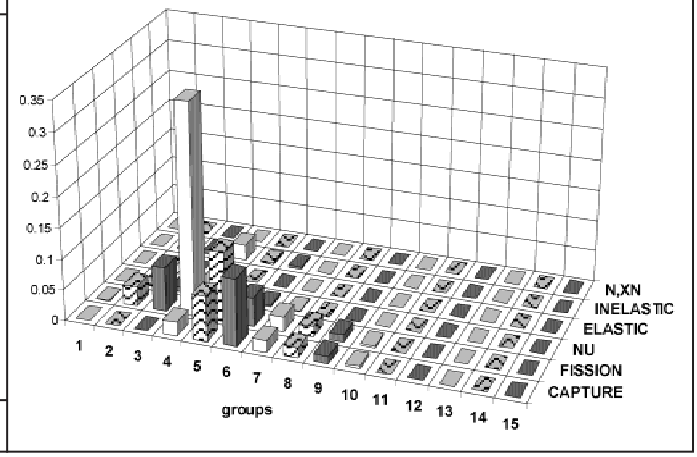

*Uncertainties (%).
[a]High-energy group boundary.
[b]Total obtained as the square root of the sum of the squares of individual contributions in row or column.
[c]Read as 4.98×10^{-1}.

TABLE XXIII

$\Delta\rho^{cycle}$ (1 yr)—Uncertainties by Isotope—Direct Effect of $\delta\sigma$*

Isotope	σ_{cap}	σ_{fiss}	ν	σ_{el}	σ_{inel}	$\sigma_{n,2n}$	Total[a]
^{238}Pu	1.1	14.3	2.9	—	0.3	—	14.6
^{239}Pu	0.6	6.0	1.4	—	0.5	—	6.2
^{240}Pu	0.1	0.7	0.2	—	—	—	0.7
^{241}Pu	0.6	4.1	0.5	—	0.1	—	4.2
^{242}Pu	0.2	0.7	0.2	—	0.1	—	0.7
^{237}Np	2.6	6.2	1.9	—	1.5	—	7.1
^{241}Am	16.0	11.7	4.1	—	2.6	—	20.4
^{242m}Am	0.5	7.6	2.3	—	0.5	—	8.0
^{243}Am	7.6	5.0	1.8	—	5.9	—	11.0
^{242}Cm	1.4	10.7	2.4	—	1.0	—	11.1
^{243}Cm	—	0.2	—	—	—	—	0.2
^{244}Cm	1.6	14.1	2.3	—	0.8	—	14.4
^{245}Cm	0.1	3.2	0.6	—	0.1	—	3.2
^{246}Cm	—	0.1	—	—	—	—	0.1
^{56}Fe	—	—	—	—	—	—	—
^{57}Fe	—	—	—	—	—	—	—
^{52}Cr	—	—	—	—	—	—	—
^{58}Ni	—	—	—	—	—	—	—
Zr	—	—	—	—	—	—	—
^{15}N	—	—	—	—	—	—	—
Pb	—	—	—	—	—	—	—
Bi	—	—	—	—	—	—	—
Fission product	1.0	—	—	—	1.8	—	2.1
Total[a]	18.1	29.0	7.2	—	7.0	—	35.6

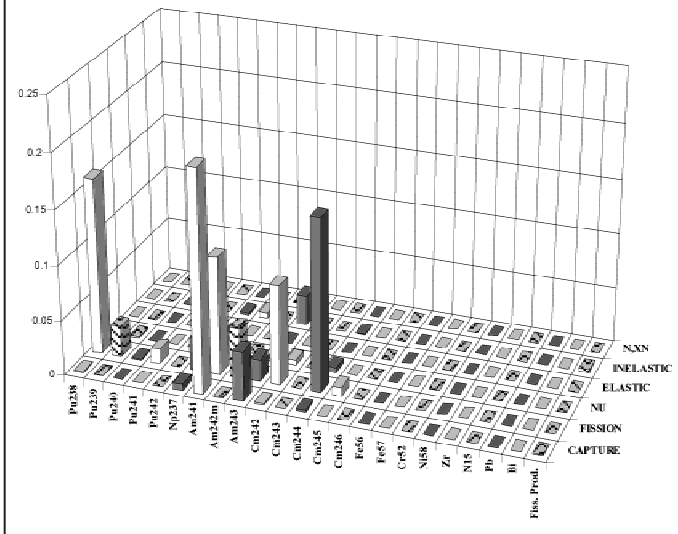

*Uncertainties (%).
[b]Total obtained as the square root of the sum of the squares of individual contributions in row or column.

TABLE XXIV

$\Delta\rho^{cycle}$ (1 yr)—Uncertainties by Isotope—Direct Effect of δn*

Isotope	σ_{cap}	σ_{fiss}	$\sigma_{n,2n}$	Total[a]
^{238}Pu	0.01	0.03	—	0.04
^{239}Pu	0.03	0.08	—	0.09
^{240}Pu	0.10	—	—	0.10
^{241}Pu	0.07	0.14	—	0.16
^{242}Pu	0.01	—	—	0.01
^{237}Np	0.20	0.01	—	0.20
^{241}Am	1.30	0.56	—	1.42
^{242m}Am	0.05	0.13	—	0.14
^{243}Am	1.43	0.60	—	1.55
^{242}Cm	0.01	0.02	—	0.02
^{244}Cm	3.96	0.49	0.01	3.99
^{245}Cm	0.30	1.97	—	2.00
Total[a]	4.43	2.20	0.01	4.95

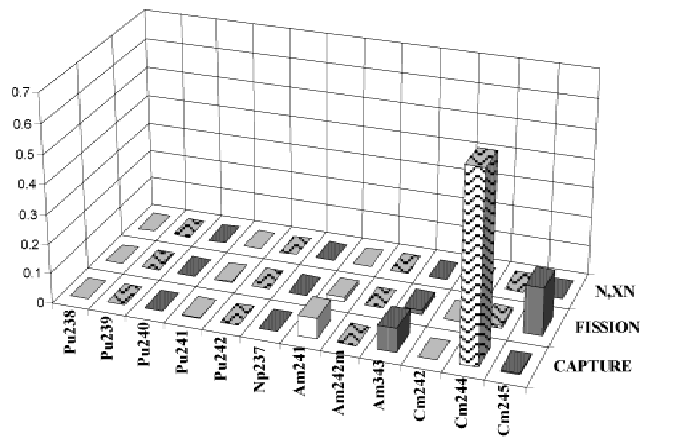

*Uncertainties (%).
[a]Total obtained as the square root of the sum of the squares of individual contributions in row or column.

IV.H. Transmutation Potential of ^{238}Pu, ^{241}Am, ^{242m}Am, ^{243}Am, ^{242}Cm, ^{244}Cm, and ^{245}Cm

The variation of the nuclide density over one irradiation cycle (or 1 yr), for example, can be taken as an indicator of the potential of a dedicated core to transmute that nuclide. A full sensitivity analysis, according to the formulation of Sec. II.B.3, has been performed for selected nuclei: ^{238}Pu, ^{241}Am, ^{242m}Am, ^{243}Am, ^{242}Cm, ^{244}Cm, and ^{245}Cm. The nuclide density variation for these isotopes for a 1-yr irradiation at full power was given in Table II.

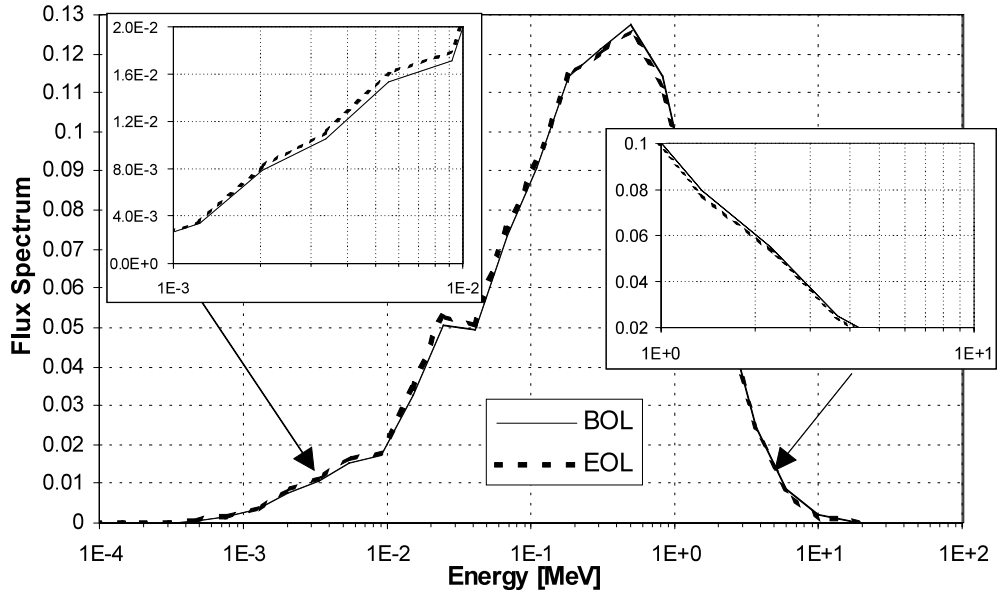

Fig. 10. Flux spectrum in the cell at BOL and after 1-yr irradiation (EOL).

TABLE XXV

One-Group Cross-Section Evolution in Time

	Fission		Capture	
	BOL	EOL[a]	BOL	EOL[a]
^{237}Np	3.90E−1[b]	3.80E−1	1.23E+0	1.26E+0
^{239}Pu	1.71E+0	1.72E+0	3.83E−1	3.93E−1
^{240}Pu	4.46E−1	4.37E−1	4.44E−1	4.54E−1
^{241}Pu	2.25E+0	2.27E+0	4.76E−1	4.81E−1
^{242}Pu	3.23E−1	3.16E−1	3.76E−1	3.85E−1
^{241}Am	3.17E−1	3.10E−1	1.59E+0	1.62E+0
^{242m}Am	2.80E+0	2.83E+0	4.16E−1	4.23E−1
^{242f}Am	2.82E+0	2.85E+0	5.17E−1	5.23E−1
^{243}Am	2.50E−1	2.44E−1	1.35E+0	1.37E+0
^{242}Cm	6.71E−1	6.60E−1	3.83E−1	3.94E−1
^{243}Cm	2.93E+0	2.96E+0	1.63E−1	1.68E−1
^{244}Cm	5.11E−1	5.00E−1	4.37E−1	4.45E−1
^{245}Cm	2.40E+0	2.42E+0	2.56E−1	2.62E−1

[a]EOL (1 yr).
[b]Read as 3.90×10^{-1}.

The major contributions to the uncertainty associated with these variations due to data (essentially cross sections) uncertainties are summarized in Table XXIX. Once more as expected, the capture and fission cross sections of ^{241}Am and ^{243}Am have significant effects (overall uncertainty on the nuclei density variation: ~20%). The case of ^{245}Cm is very interesting because there is an indication of a potential uncertainty of a factor of ~2 on the ^{245}Cm buildup at the end of the 1-yr irradiation, due in particular to the ^{244}Cm capture cross-section assumed uncertainty.

This result is relevant, since ^{244}Cm is the gateway to higher mass isotopes, some of them with potentially relevant effects on the fuel cycle (e.g., ^{252}Cf, strong neutron emitter by spontaneous fission). These higher mass isotopes do not appear in our present study, limited to one cycle irradiation (1 yr), but will be very relevant in the case of multiple recycle of the MA fuel.

TABLE XXVI

Decay Heat and Its Evolution in Time*

	Discharge[a]	500 s	1000 s	3000 s	1 h	12 h	1 day	10 days
Light elements	6.98E+4[b]	5.72E+4	5.46E+4	5.24E+4	5.19E+4	4.21E+4	4.14E+4	3.89E+4
Heavy elements	5.64E+6	5.51E+6	5.40E+6	5.14E+6	5.09E+6	4.85E+6	4.77E+6	4.38E+6
Fission products	1.93E+7	6.36E+6	5.39E+6	3.84E+6	3.61E+6	1.70E+6	1.39E+6	6.93E+5
Total	2.51E+7	1.19E+7	1.08E+7	9.03E+6	8.76E+6	6.59E+6	6.20E+6	5.11E+6

*Decay heat (W).
[a]EOL (2 yr).
[b]Read as 6.98×10^4.

TABLE XXVII

Decay Heat—Heavy Element Breakdown by Isotope*

	Discharge[a]	500 s	1000 s	3000 s	1 h	12 h	1 day	10 days
U	7.63E+0[b]	7.62E+0	7.61E+0	7.59E+0	7.58E+0	7.29E+0	7.01E+0	3.71E+0
Np	3.05E+5	3.04E+5	3.04E+5	3.01E+5	3.01E+5	2.58E+5	2.19E+5	1.15E+4
Pu	9.59E+4	9.58E+4	9.56E+4	9.50E+4	9.49E+4	8.93E+4	8.81E+4	8.85E+4
Am	9.08E+5	7.73E+5	6.65E+5	4.08E+5	3.66E+5	1.73E+5	1.34E+5	7.83E+4
Cm	4.33E+6	4.33E+6	4.33E+6	4.33E+6	4.33E+6	4.33E+6	4.33E+6	4.20E+6
Bk	1.37E−3	1.35E−3	1.33E−3	1.26E−3	1.26E−3	7.09E−4	6.58E−4	6.41E−4
Cf	2.16E−4	2.16E−4	2.16E−4	2.16E−4	2.16E−4	2.17E−4	2.17E−4	2.22E−4
Total	5.64E+6	5.51E+6	5.40E+6	5.14E+6	5.09E+6	4.85E+6	4.77E+6	4.38E+6

*Decay heat (W).
[a]EOL (2 yr).
[b]Read as 7.63×10^0.

TABLE XXVIII

Decay Heat—Relative Contribution of Heavy Isotopes and Fission Products at Different Cooling Times*

	Discharge[a]	500 s	1000 s	3000 s	1 h	12 h	1 day	10 days
ADS								
Heavy elements	23	46	50	57	58	74	77	86
Fission products	77	53	50	43	41	26	22	14
Superphenix								
Heavy elements	8.9	NA	20.2	22.3	22.5	32.3	34.5	22.8
Fission products	89.7	NA	74.6	72.6	72.3	63.7	62.1	73.2

*Relative contribution (%).
[a]EOL (2 yr).

The uncertainties related to their buildup have to be carefully assessed in performing full-fuel-cycle and transmutation scenario studies.

IV.I. The Peak Power Value and Its Uncertainty

The system considered for the present analysis is subcritical by ~5% $\Delta K/K$, and as expected, the radial power shape in the core shows a marked gradient, which gives rise to a maximum-to-average power ratio of ~2.9 (see Table II). This parameter is important because the cooling system of the system, for example, should account for the power gradient and its possible evolution in time.

We have performed the uncertainty analysis using the perturbation formulation of Sec. II.B.2, for the following reaction rate ratio:

TABLE XXIX

Uncertainties on the Nuclear Density Variation of ^{238}Pu, ^{241}Am, ^{242m}Am, ^{243}Am, ^{242}Cm, ^{244}Cm, and ^{245}Cm*

Isotope	Uncertainty due to:								Total
^{238}Pu	^{237}Np		^{238}Pu		^{241}Am		^{242}Cm		
	Capture	Fission	Capture	Fission	Capture	Fission	Capture	Fission	
	3.67	0.12	0.19	0.61	6.31	0.04	0.06	0.09	7.33
^{241}Am	^{241}Am								
	Capture	Fission							
	11.06	10.31							15.12
^{242m}Am	^{241}Am		^{242m}Am						
	Capture	Fission	Capture	Fission					
	15.70	0.15	0.83	2.45					15.91
^{243}Am	^{242}Pu	^{243}Am							
	Capture	Capture	Fission						
	0.22	10.66	10.94						15.28
^{242}Cm	^{241}Am		^{242}Cm						
	Capture	Fission	Capture	Fission					
	12.54	0.15	0.17	0.27					12.54
^{244}Cm	^{243}Am		^{244}Cm						
	Capture	Fission	Capture	Fission	$(n,2n)$				
	23.48	0.20	4.98	8.75	0.20				25.55
^{245}Cm	^{243}Am		^{244}Cm			^{245}Cm			
	Capture	Fission	Capture	Fission	$(n,2n)$	Capture	Fission	$(n,2n)$	
	4.82	0.03	72.33	1.71	0.04	5.48	36.10	0.03	81.19

*Values are in percent.

$$P^{Max} = \frac{\langle \underline{\Sigma}_f, \underline{\Phi} \rangle_{r=r_{Max}}}{\langle \underline{\Sigma}_f, \underline{\Phi} \rangle_{Average}} \quad , \tag{39}$$

where $r = r_{Max}$ is the spatial position where the maximum power is observed.

The results are shown in Tables XXX and XXXI. The major contribution to uncertainty (total value $\pm 20.5\%$) is given by ^{241}Am and ^{243}Am capture and fission cross sections, ^{244}Cm fission, and ^{243}Am inelastic cross sections. Also ^{56}Fe, Pb, and Bi inelastic cross-section uncertainties make a significant contribution.

An inspection of the sign associated with the sensitivity coefficients shows that for all isotopes, the capture sensitivity coefficients are positive and those for fission are negative over the entire energy range. The inelastic cross-section sensitivity coefficients are positive down to a few hundred kilovolts. In fact, an increase of the captures [or a reduction of $(\nu - 1)\sigma_f$] means an increase

TABLE XXX

Power Peak—Uncertainties by Group*

Group	(MeV)[a]	σ_{cap}	σ_{fiss}	ν	σ_{el}	σ_{inel}	$\sigma_{n,2n}$	Total[b]
1	19.6	—	0.4	0.1	—	0.4	—	0.5
2	6.07	0.1	3.9	1.3	0.2	3.5	—	5.4
3	2.23	0.2	5.8	1.9	0.2	3.3	—	6.9
4	1.35	3.6	11.0	3.0	1.6	6.0	—	13.5
5	4.98E−1[c]	6.5	2.9	0.6	0.6	1.6	—	7.3
6	1.83E−1	7.9	2.4	0.5	0.4	1.5	—	8.4
7	6.74E−2	3.2	1.8	0.5	0.2	0.3	—	3.8
8	2.48E−2	2.9	1.6	0.3	—	0.3	—	3.4
9	9.12E−3	2.4	1.5	0.2	0.1	—	—	2.9
10	2.04E−3	1.6	0.6	0.1	0.1	—	—	1.7
11	4.54E−4	0.3	0.1	—	0.1	—	—	0.3
12	2.26E−5	—	—	—	—	—	—	—
13	4.00E−6	—	—	—	—	—	—	—
14	5.40E−7	—	—	—	—	—	—	—
15	1.00E−7	—	—	—	—	—	—	—
Total[b]		12.0	13.9	3.9	1.8	8.0	—	20.5

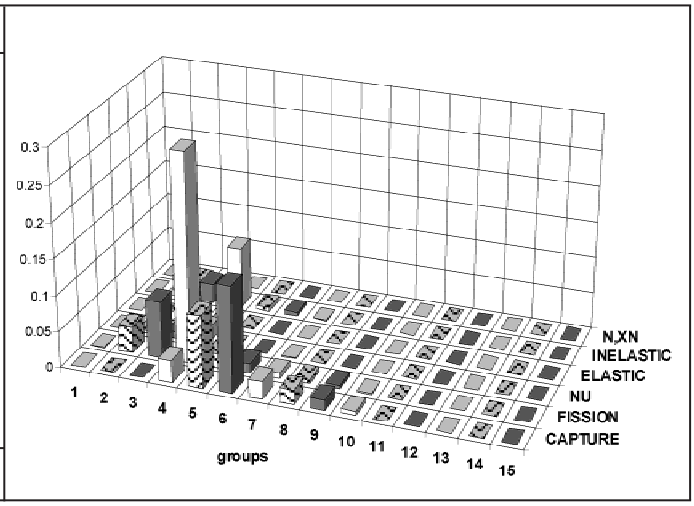

*Uncertainties (%).
[a]High-energy group boundary.
[b]Total obtained as the square root of the sum of the squares of individual contributions in row or column.
[c]Read as 4.98×10^{-1}.

of the subcritical level and, as consequence, a more peaked behavior of the power shape. As for the inelastic cross sections and in view of the sharp slope in energy of the adjoint flux (see Fig. 6), an increase of σ_{in} will transfer neutrons to lower importance energy regions, with a consequent decrease in the reactivity level and increase of the power gradient. Finally, note once more the significant contribution of the ^{243}Am inelastic cross section

TABLE XXXI

Power Peak—Uncertainties by Isotope*

Isotope	σ_{cap}	σ_{fiss}	ν	σ_{el}	σ_{inel}	$\sigma_{n,2n}$	Total[a]
^{238}Pu	0.1	0.8	0.2	—	—	—	0.8
^{239}Pu	0.3	3.7	0.8	—	0.3	—	3.8
^{240}Pu	0.4	1.3	0.4	—	0.1	—	1.4
^{241}Pu	0.3	2.2	0.2	—	0.1	—	2.3
^{242}Pu	0.1	0.4	0.1	—	—	—	0.4
^{237}Np	1.9	4.9	1.5	—	1.1	—	5.6
^{241}Am	10.3	7.9	2.7	—	1.7	—	13.4
^{242m}Am	—	0.7	0.2	—	—	—	0.7
^{243}Am	5.8	4.2	1.5	—	4.7	—	8.7
^{242}Cm	—	—	—	—	—	—	—
^{243}Cm	—	0.3	0.1	—	—	—	0.4
^{244}Cm	1.0	7.7	1.3	—	0.5	—	7.9
^{245}Cm	0.1	3.0	0.6	—	0.1	—	3.1
^{246}Cm	—	—	—	—	—	—	—
^{56}Fe	0.2	—	—	0.5	3.9	—	3.9
^{57}Fe	—	—	—	—	0.5	—	0.5
^{52}Cr	—	—	—	0.1	0.2	—	0.2
^{58}Ni	—	—	—	—	—	—	—
Zr	0.2	—	—	0.4	0.6	—	0.7
^{15}N	—	—	—	1.6	0.1	—	1.6
Pb	0.2	—	—	0.2	3.0	—	3.0
Bi	0.2	—	—	0.3	3.6	—	3.6
Total[a]	12.0	13.9	3.9	1.8	8.0	—	20.5

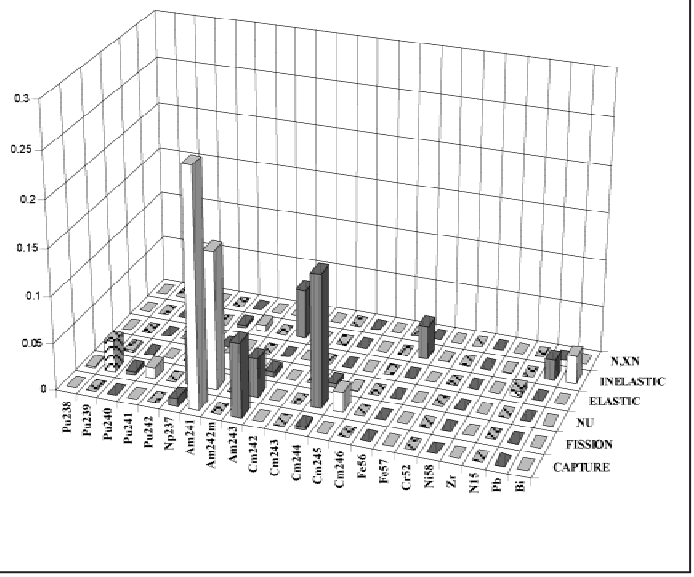

*Uncertainties (%).
[a]Total obtained as the square root of the sum of the squares of individual contributions in row or column.

TABLE XXXII

Main Parameters of the Reference System

Calculation	φ^*	Maximum dpa[a] ($s^{-1} \times cm^{-3}$)	Maximum He Production[a] ($s^{-1} \times cm^{-3}$)	Maximum H Production[a] ($s^{-1} \times cm^{-3}$)	Maximum (He production)/dpa[a]
150 MeV—Reference	1.20	2.58E+16	7.31E+15	7.31E+16	0.28
20 MeV—Option A	1.18	2.58E+16	6.15E+15	6.77E+16	0.24
20 MeV—Option B	1.29	2.59E+16	9.28E+15	7.49E+16	0.36

[a]See text for description.
[b]Read as 2.58×10^{16}.

already indicated previously in the case of other integral parameters (k_{eff}, etc.).

V. PARAMETERS WITH HIGH-ENERGY ($E > 20$ MeV) DATA DEPENDENCE

A few of the parameters considered in our study can show a significant sensitivity to data at energy $E >$ 20 MeV. This is the case of φ^*, Max He and H production, Max dpa, and Max (He production)/dpa.

The nominal values given in Table III were calculated using the cross-section library with upper energy boundary at 20 MeV and with the high-energy neutron source ($E > 20$ MeV, calculated with MCNPX) redistributed on the energy range from 0 to 20 MeV. We call this calculation option A. The availability of a multigroup library extended to 150 MeV, based on the data evaluated at Los Alamos National Laboratory (see Sec. II.C), allowed us to check this approximation. Another approximation was also checked, i.e., a calculation with the upper energy boundary still at 20 MeV but with the high-energy neutron source at $E > 20$ MeV added to the first group of the energy structure between 0 and 20 MeV (option B). The three calculations (multigroup extended to 150 MeV taken as reference; multigroup up to 20 MeV: options A and B) are shown in Table XXXII.

A better agreement is shown with respect to the reference when option A is used. Option B tends to provide overestimated values, giving too much weight to the neutrons at ~20 MeV. This effect is made evident by a comparison of the spectrum at high energy ($E > 1$ MeV) obtained with the three calculations (see Fig. 11).

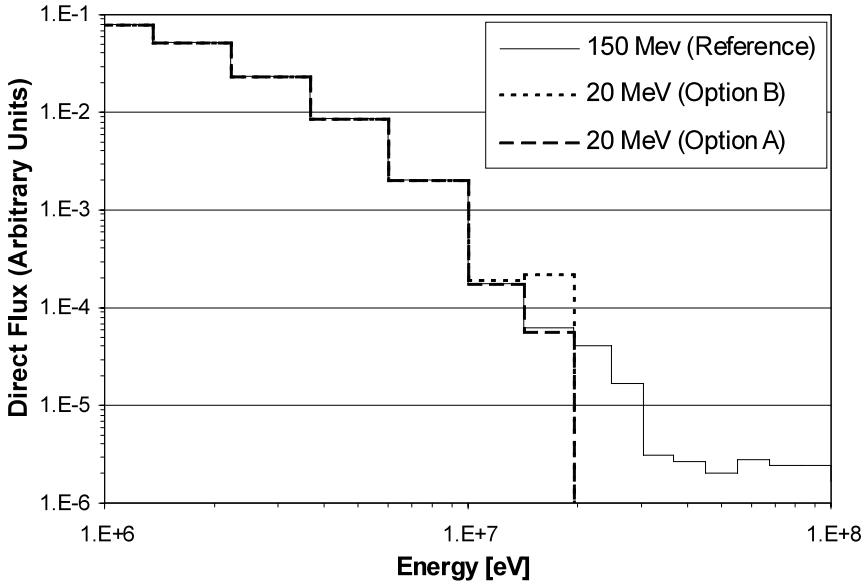

Fig. 11. Flux spectrum above 1 MeV as obtained with three different calculations to account for high-energy ($E > 20$ MeV) neutrons (see text for details). The three spectra have been normalized to the same integral value over the full energy range.

The extension of the multigroup cross-section library up to 150 MeV has a significant impact on some parameters like the Max He production and, consequently, on the Max (He production)/dpa in the structures.

On the other hand, the multigroup library extension up to 150 MeV has been shown to have a negligible impact on parameters like k_{eff}, reactivity coefficients, reactivity loss during irradiation, power peak, etc.

Finally, for the sensitivity/uncertainty analysis for φ^*, Max He and H production, Max dpa, and Max (He production)/dpa, the reference library (i.e., multigroup extended to 150 MeV) has been adopted.

As for uncertainties, the uncertainties associated with the cross sections extended to 150 MeV have been used in a 17-group structure, adding two more groups to the 15-group structure corresponding to the reference library with upper limit at $E = 19.64$ MeV (Tables IV, V, and VI): the energy boundaries of these two groups are 150 to 55.2 MeV (group 1 of the new 17-group structure) and 55.2 to 19.64 MeV (group 2). As for the uncertainties related to the cross sections, the uncertainties of group 1 in the usual 15-group structure have been multiplied by a factor of 3 in group 1 and by a factor of 2 in group 2 of the new 17-group structure to account for the larger spread of data observed at higher energy.

V.A. The φ^* and Its Uncertainty

The formulation given in Sec. II.B.5 has been used to derive sensitivities and uncertainties. The uncertainty values by energy group and by isotope and reaction type are given in Tables XXXIII and XXXIV.

In general, due to the nature of φ^* and its expression as a ratio, the impact of cross-section uncertainties is relatively small (total uncertainty value with no energy correlation less than ±3%). The impact of high-energy data, $E > 20$ MeV (in particular, σ_{in} and $\sigma_{n,2n}$ of Pb and Bi), is limited.

V.B. Max dpa, Max He and H Production, Max (He Production)/dpa

Among the parameters considered, the four most sensitive to high-energy data are shown in Tables XXXV through XLII. These tables give the indirect (i.e., related to flux changes) components of the uncertainty. However, for the case of the Max He and H production, a significant part of the uncertainty comes from direct effects, i.e., the effects due to the uncertainties of (n, α) and (n, p) cross sections in the structures. We have assumed a ±20% uncertainty for all these cross sections. The final uncertainty value is obtained by the linear sum of the direct and the indirect effects components of the uncertainty (see Table XLIII).

The total uncertainty is significant and obviously has an impact on the Max (He production)/dpa, which is relevant in the assessment of material damage, and for characterizing appropriate irradiation conditions, in particular in spallation-source-driven systems (see, for example, Ref. 28).

TABLE XXXIII

φ^*—Uncertainties by Group*

Group	(MeV)[a]	σ_{cap}	σ_{fiss}	ν	σ_{el}	σ_{inel}	$\sigma_{n,2n}$	Total[b]
1	150	—	0.03	0.01	—	0.08	—	0.08
2	55.2	0.01	0.05	0.02	—	0.82	0.36	0.90
3	19.6	0.01	0.05	0.02	0.02	0.53	0.49	0.72
4	6.07	0.01	0.03	0.01	0.14	0.96	—	0.97
5	2.23	0.02	0.19	0.06	0.20	1.00	—	1.04
6	1.35	0.33	0.88	0.24	0.33	0.95	—	1.40
7	4.98E−1[c]	0.72	0.30	0.06	0.09	0.19	—	0.81
8	1.83E−1	0.92	0.27	0.06	0.06	0.17	—	0.98
9	6.74E−2	0.41	0.22	0.07	0.02	0.02	—	0.47
10	2.48E−2	0.37	0.20	0.04	0.02	—	—	0.42
11	9.12E−3	0.32	0.20	0.03	0.01	—	—	0.37
12	2.04E−3	0.20	0.08	0.02	0.01	—	—	0.21
13	4.54E−4	0.04	0.01	—	—	—	—	0.04
14	2.26E−5	—	—	—	—	—	—	—
15	4.00E−6	—	—	—	—	—	—	—
16	5.40E−7	—	—	—	—	—	—	—
17	1.00E−7	—	—	—	—	—	—	—
Total[b]		1.39	1.06	0.27	0.43	1.82	0.96	2.74

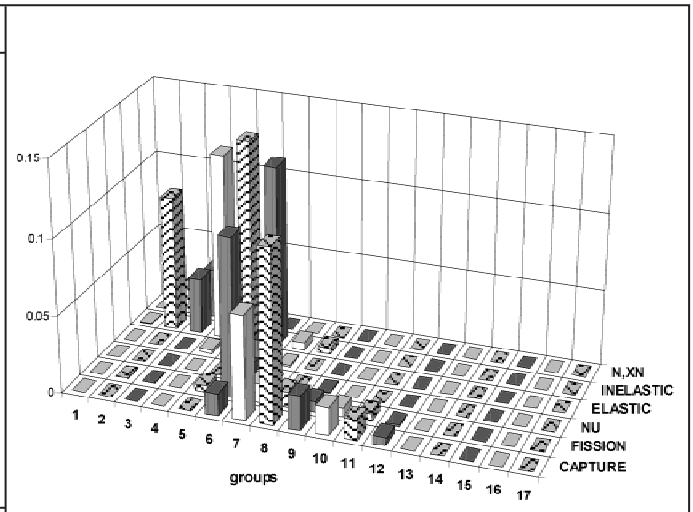

*Uncertainties (%).
[a]High-energy group boundary.
[b]Total obtained as the square root of the sum of the squares of individual contributions in row or column.
[c]Read as 4.98×10^{-1}.

TABLE XXXIV

φ^*—Uncertainties by Isotope*

Isotope	σ_{cap}	σ_{fiss}	ν	σ_{el}	σ_{inel}	$\sigma_{n,2n}$	Total[a]
^{238}Pu	0.01	0.08	0.02	—	—	—	0.08
^{239}Pu	0.04	0.37	0.09	—	0.02	—	0.39
^{240}Pu	0.04	0.10	0.03	—	0.01	—	0.12
^{241}Pu	0.03	0.26	0.03	—	—	—	0.26
^{242}Pu	0.01	0.03	0.01	—	—	—	0.03
^{237}Np	0.23	0.37	0.11	—	0.08	—	0.46
^{241}Am	1.18	0.48	0.17	—	0.12	—	1.29
^{242m}Am	0.01	0.08	0.02	—	—	—	0.08
^{243}Am	0.67	0.25	0.09	—	0.41	—	0.83
^{242}Cm	—	—	—	—	—	—	—
^{243}Cm	—	0.04	0.01	—	—	—	0.04
^{244}Cm	0.12	0.58	0.10	—	0.02	—	0.61
^{245}Cm	0.01	0.34	0.07	—	—	—	0.35
^{246}Cm	—	—	—	—	—	—	—
^{56}Fe	0.03	—	—	0.15	0.24	—	0.28
^{57}Fe	—	—	—	—	0.03	—	0.03
^{52}Cr	0.01	—	—	0.04	0.01	—	0.04
^{58}Ni	—	—	—	—	—	—	—
Zr	0.02	—	—	0.06	0.02	—	0.07
^{15}N	0.01	—	—	0.16	0.02	—	0.16
Pb	0.06	—	—	0.23	1.20	0.54	1.33
Bi	0.08	—	—	0.28	1.27	0.79	1.52
Total[a]	1.39	1.06	0.27	0.43	1.82	0.96	2.74

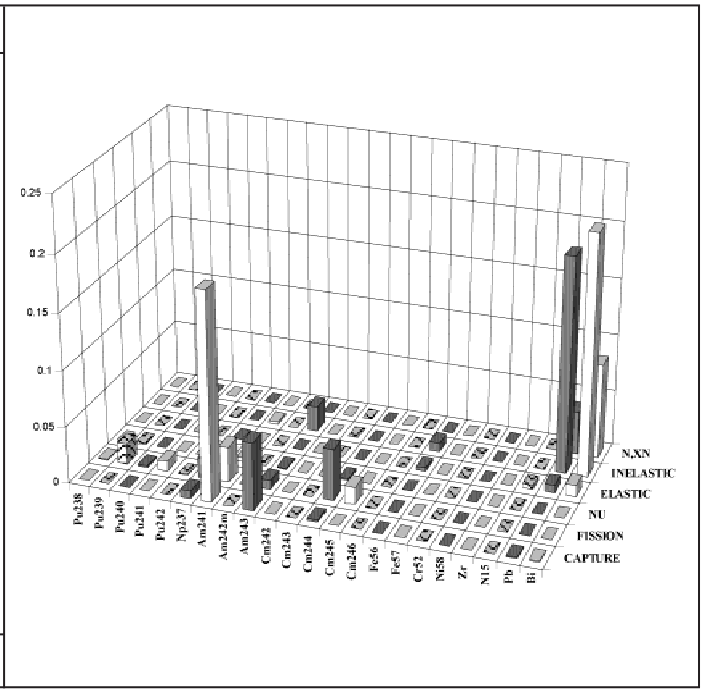

*Uncertainties (%).
[a]Total obtained as the square root of the sum of the squares of individual contributions in row or column.

TABLE XXXV

Maximum dpa—Uncertainties by Group*

Group	(MeV)[a]	σ_{cap}	σ_{fiss}	ν	σ_{el}	σ_{inel}	$\sigma_{n,2n}$	Total[b]
1	150	—	—	—	—	0.1	—	0.1
2	55.2	—	—	—	—	1.0	0.3	1.0
3	19.6	0.1	0.5	0.2	—	1.1	0.2	1.2
4	6.07	0.1	5.5	1.8	0.4	7.9	—	9.8
5	2.23	0.4	8.2	2.7	0.8	6.4	—	10.8
6	1.35	5.0	15.9	4.2	2.4	9.1	—	19.6
7	4.98E−1[c]	8.8	4.1	0.8	1.3	2.0	—	10.0
8	1.83E−1	10.5	3.3	0.7	0.8	2.0	—	11.3
9	6.74E−2	4.3	2.5	0.8	0.3	0.4	—	5.1
10	2.48E−2	3.8	2.2	0.4	0.3	0.2	—	4.4
11	9.12E−3	3.2	2.1	0.3	0.1	—	—	3.8
12	2.04E−3	2.0	0.9	0.2	—	—	—	2.2
13	4.54E−4	0.3	0.1	—	—	—	—	0.4
14	2.26E−5	—	—	—	—	—	—	—
15	4.00E−6	—	—	—	—	—	—	—
16	5.40E−7	—	—	—	—	—	—	—
17	1.00E−7	—	—	—	—	—	—	—
Total[b]		16.1	19.9	5.5	3.0	14.1	0.5	29.9

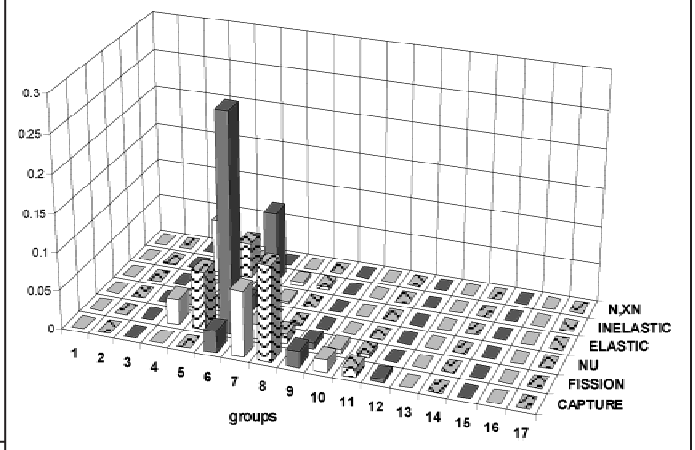

*Uncertainties (%).
[a]High-energy group boundary.
[b]Total obtained as the square root of the sum of the squares of individual contributions in row or column.
[c]Read as 4.98×10^{-1}.

TABLE XXXVI

Maximum dpa—Uncertainties by Isotope*

Isotope	σ_{cap}	σ_{fiss}	ν	σ_{el}	σ_{inel}	$\sigma_{n,2n}$	Total[a]
^{238}Pu	0.1	1.1	0.2	—	—	—	1.1
^{239}Pu	0.4	5.2	1.2	—	0.4	—	5.4
^{240}Pu	0.5	1.8	0.5	—	0.2	—	2.0
^{241}Pu	0.4	3.1	0.3	—	0.1	—	3.2
^{242}Pu	0.2	0.5	0.2	—	0.1	—	0.6
^{237}Np	2.5	7.1	2.1	—	1.6	—	8.0
^{241}Am	13.8	11.3	3.9	—	2.5	—	18.4
^{242m}Am	0.1	1.0	0.3	—	0.1	—	1.0
^{243}Am	7.7	6.0	2.1	—	6.6	—	12.0
^{242}Cm	—	—	—	—	—	—	—
^{243}Cm	—	0.5	0.1	—	—	—	0.5
^{244}Cm	1.3	11.1	1.9	—	0.8	—	11.3
^{245}Cm	0.1	4.2	0.8	—	0.1	—	4.3
^{246}Cm	—	—	—	—	—	—	—
^{56}Fe	0.3	—	—	0.6	5.5	—	5.6
^{57}Fe	—	—	—	—	0.6	—	0.6
^{52}Cr	0.1	—	—	0.1	0.3	—	0.3
^{58}Ni	—	—	—	—	—	—	—
Zr	0.3	—	—	0.3	0.9	—	1.0
^{15}N	—	—	—	2.1	0.1	—	2.1
Pb	0.3	—	—	1.3	6.8	0.2	7.0
Bi	0.4	—	—	1.5	8.1	0.4	8.3
Total[a]	16.1	19.9	5.5	3.0	14.1	0.5	29.9

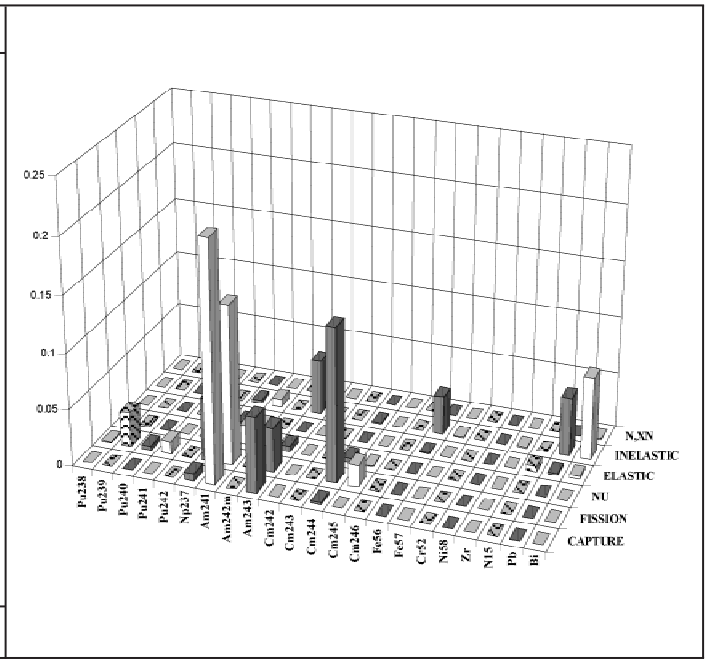

*Uncertainties (%).
[a]Total obtained as the square root of the sum of the squares of individual contributions in row or column.

TABLE XXXVII

Maximum He Production—Uncertainties by Group*

Group	(MeV)[a]	σ_{cap}	σ_{fiss}	ν	σ_{el}	σ_{inel}	$\sigma_{n,2n}$	Total[b]
1	150	—	—	—	0.1	4.9	—	4.9
2	55.2	0.1	—	—	0.2	21.2	5.7	21.9
3	19.6	0.1	0.1	0.1	0.7	13.2	32.8	35.4
4	6.07	—	2.3	0.7	0.1	3.5	—	4.2
5	2.23	0.1	3.5	1.1	0.3	2.1	—	4.2
6	1.35	1.9	6.7	1.7	0.9	3.2	—	7.9
7	4.98E−1[c]	3.5	1.7	0.3	0.5	0.7	—	4.0
8	1.83E−1	4.2	1.4	0.3	0.3	0.8	—	4.5
9	6.74E−2	1.7	1.0	0.3	0.1	0.1	—	2.0
10	2.48E−2	1.5	0.9	0.2	0.1	0.1	—	1.8
11	9.12E−3	1.3	0.9	0.1	—	—	—	1.6
12	2.04E−3	0.8	0.3	0.1	—	—	—	0.9
13	4.54E−4	0.1	0.1	—	—	—	—	0.1
14	2.26E−5	—	—	—	—	—	—	—
15	4.00E−6	—	—	—	—	—	—	—
16	5.40E−7	—	—	—	—	—	—	—
17	1.00E−7	—	—	—	—	—	—	—
Total[b]		6.4	8.3	2.3	1.4	13.5	40.0	43.6

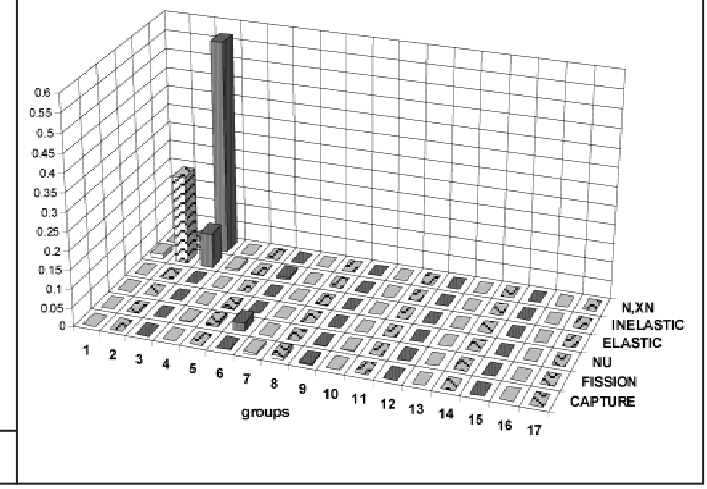

*Uncertainties (%).
[a]High-energy group boundary.
[b]Total obtained as the square root of the sum of the squares of individual contributions in row or column.
[c]Read as 4.98×10^{-1}.

TABLE XXXVIII

Maximum He Production—Uncertainties by Isotope*

Isotope	σ_{cap}	σ_{fiss}	ν	σ_{el}	σ_{inel}	$\sigma_{n,2n}$	Total[a]
^{238}Pu	—	0.4	0.1	—	—	—	0.5
^{239}Pu	0.2	2.2	0.5	—	0.2	—	2.2
^{240}Pu	0.2	0.8	0.2	—	0.1	—	0.8
^{241}Pu	0.2	1.3	0.1	—	—	—	1.3
^{242}Pu	0.1	0.2	0.1	—	—	—	0.2
^{237}Np	1.0	3.0	0.9	—	0.6	—	3.3
^{241}Am	5.5	4.7	1.6	—	0.9	—	7.5
^{242m}Am	—	0.4	0.1	—	—	—	0.4
^{243}Am	3.1	2.5	0.9	—	2.5	—	4.7
^{242}Cm	—	—	—	—	—	—	—
^{243}Cm	—	0.2	—	—	—	—	0.2
^{244}Cm	0.5	4.6	0.8	—	0.3	—	4.7
^{245}Cm	—	1.7	0.3	—	—	—	1.8
^{246}Cm	—	—	—	—	—	—	—
^{56}Fe	0.1	—	—	0.2	2.0	—	2.0
^{57}Fe	—	—	—	—	0.2	—	0.2
^{52}Cr	—	—	—	—	0.3	—	0.3
^{58}Ni	—	—	—	—	—	—	—
Zr	0.1	—	—	0.1	0.5	—	0.5
^{15}N	—	—	—	0.8	0.4	—	0.9
Pb	0.1	—	—	0.8	8.5	22.2	23.8
Bi	0.2	—	—	0.9	10.0	33.3	34.8
Total[a]	6.4	8.3	2.3	1.4	13.5	40.0	43.6

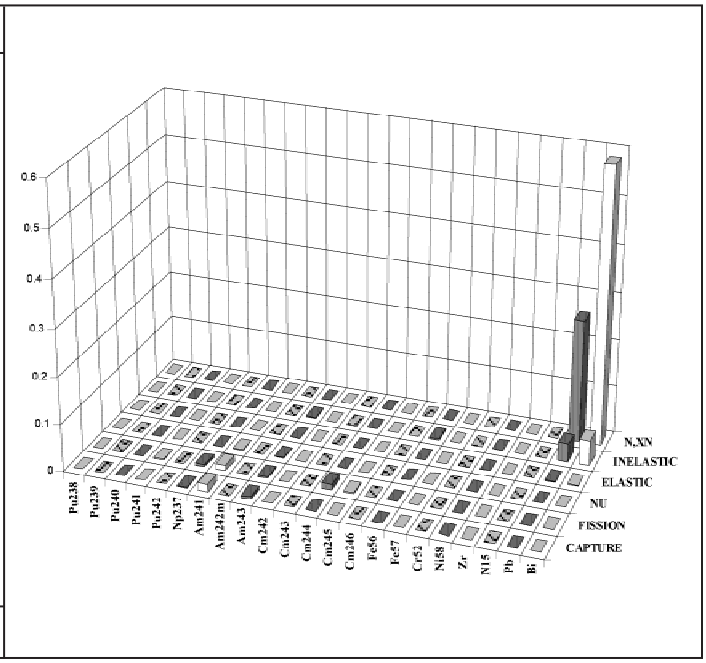

*Uncertainties (%).
[a]Total obtained as the square root of the sum of the squares of individual contributions in row or column.

TABLE XXXIX

Maximum H Production—Uncertainties by Group*

Group	(MeV)[a]	σ_{cap}	σ_{fiss}	ν	σ_{el}	σ_{inel}	$\sigma_{n,2n}$	Total[b]
1	150	—	—	—	—	1.8	—	1.8
2	55.2	—	—	—	0.1	6.5	1.2	6.6
3	19.6	0.1	0.4	0.1	0.2	5.3	8.6	10.1
4	6.07	0.1	4.3	1.4	0.2	12.6	—	13.4
5	2.23	0.3	6.7	2.2	0.5	4.6	—	8.4
6	1.35	3.7	12.9	3.4	1.7	6.2	—	15.3
7	4.98E−1[c]	6.7	3.3	0.6	1.0	1.4	—	7.7
8	1.83E−1	8.1	2.6	0.6	0.6	1.6	—	8.7
9	6.74E−2	3.3	2.0	0.6	0.3	0.3	—	4.0
10	2.48E−2	3.0	1.8	0.3	0.2	0.2	—	3.5
11	9.12E−3	2.5	1.7	0.3	0.1	—	—	3.0
12	2.04E−3	1.6	0.7	0.1	—	—	—	1.7
13	4.54E−4	0.3	0.1	—	—	—	—	0.3
14	2.26E−5	—	—	—	—	—	—	—
15	4.00E−6	—	—	—	—	—	—	—
16	5.40E−7	—	—	—	—	—	—	—
17	1.00E−7	—	—	—	—	—	—	—
Total[b]		12.4	16.1	4.4	2.2	16.6	9.9	28.5

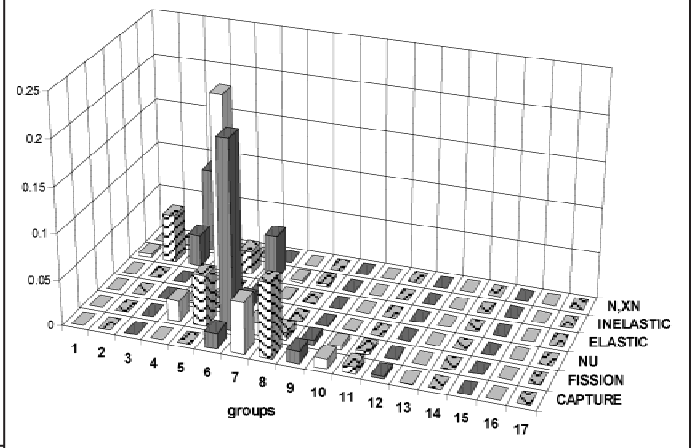

*Uncertainties (%).
[a]High-energy group boundary.
[b]Total obtained as the square root of the sum of the squares of individual contributions in row or column.
[c]Read as 4.98×10^{-1}.

TABLE XL

Maximum H Production—Uncertainties by Isotope*

Isotope	σ_{cap}	σ_{fiss}	ν	σ_{el}	σ_{inel}	$\sigma_{n,2n}$	Total[a]
^{238}Pu	0.1	0.9	0.2	—	—	—	0.9
^{239}Pu	0.3	4.2	0.9	—	0.3	—	4.3
^{240}Pu	0.4	1.5	0.4	—	0.2	—	1.6
^{241}Pu	0.3	2.5	0.3	—	0.1	—	2.5
^{242}Pu	0.1	0.4	0.1	—	0.1	—	0.5
^{237}Np	2.0	5.7	1.7	—	1.2	—	6.4
^{241}Am	10.6	9.1	3.1	—	1.8	—	14.4
^{242m}Am	0.1	0.8	0.2	—	—	—	0.8
^{243}Am	6.0	4.8	1.7	—	4.8	—	9.2
^{242}Cm	—	—	—	—	—	—	—
^{243}Cm	—	0.4	0.1	—	—	—	0.4
^{244}Cm	1.0	9.0	1.5	—	0.6	—	9.2
^{245}Cm	0.1	3.4	0.7	—	0.1	—	3.4
^{246}Cm	—	—	—	—	—	—	—
^{56}Fe	0.2	—	—	0.4	3.9	—	4.0
^{57}Fe	—	—	—	—	0.4	—	0.4
^{52}Cr	—	—	—	0.1	0.3	—	0.3
^{58}Ni	—	—	—	—	—	—	—
Zr	0.2	—	—	0.2	0.9	—	0.9
^{15}N	—	—	—	1.5	0.2	—	1.5
Pb	0.2	—	—	1.0	9.1	5.5	10.6
Bi	0.3	—	—	1.2	12.1	8.3	14.8
Total[a]	12.4	16.1	4.4	2.2	16.6	9.9	28.5

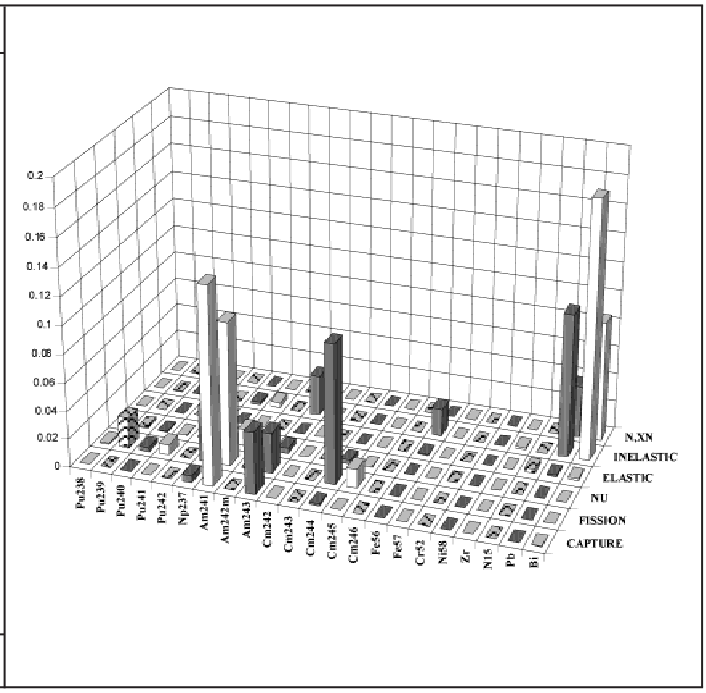

*Uncertainties (%).
[a]Total obtained as the square root of the sum of the squares of individual contributions in row or column.

TABLE XLI

Maximum (He Production)/dpa—Uncertainties by Group*

Group	(MeV)[a]	σ_{cap}	σ_{fiss}	ν	σ_{el}	σ_{inel}	$\sigma_{n,2n}$	Total[b]
1	150	—	—	—	0.1	4.8	—	4.8
2	55.2	—	0.1	—	0.2	20.1	6.4	21.1
3	19.6	—	0.7	0.2	0.7	11.6	34.0	35.9
4	6.07	0.1	3.2	1.0	0.3	4.5	—	5.6
5	2.23	0.2	4.7	1.6	0.5	4.3	—	6.6
6	1.35	3.1	9.2	2.5	1.5	5.8	—	11.7
7	4.98E−1[c]	5.2	2.4	0.5	0.8	1.3	—	6.0
8	1.83E−1	6.3	2.0	0.4	0.5	1.2	—	6.7
9	6.74E−2	2.6	1.5	0.4	0.2	0.2	—	3.0
10	2.48E−2	2.2	1.3	0.2	0.2	0.1	—	2.6
11	9.12E−3	1.9	1.2	0.2	—	—	—	2.3
12	2.04E−3	1.2	0.5	0.1	—	—	—	1.3
13	4.54E−4	0.2	0.1	—	—	—	—	0.2
14	2.26E−5	—	—	—	—	—	—	—
15	4.00E−6	—	—	—	—	—	—	—
16	5.40E−7	—	—	—	—	—	—	—
17	1.00E−7	—	—	—	—	—	—	—
Total[b]		9.6	11.5	3.2	2.0	14.1	40.4	45.5

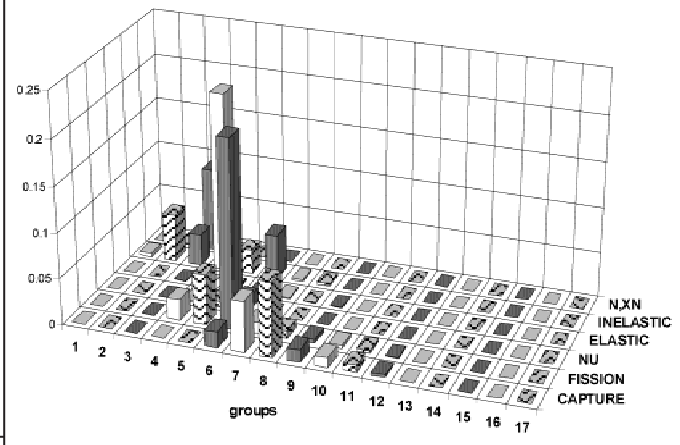

*Uncertainties (%).
[a]High-energy group boundary.
[b]Total obtained as the square root of the sum of the squares of individual contributions in row or column.
[c]Read as 4.98×10^{-1}.

TABLE XLII

Maximum (He Production)/dpa—Uncertainties by Isotope*

Isotope	σ_{cap}	σ_{fiss}	ν	σ_{el}	σ_{inel}	$\sigma_{n,2n}$	Total[a]
^{238}Pu	0.1	0.6	0.1	—	—	—	0.7
^{239}Pu	0.3	3.0	0.7	—	0.3	—	3.1
^{240}Pu	0.3	1.1	0.3	—	0.1	—	1.1
^{241}Pu	0.3	1.8	0.2	—	0.1	—	1.9
^{242}Pu	0.1	0.3	0.1	—	—	—	0.3
^{237}Np	1.5	4.0	1.2	—	1.0	—	4.6
^{241}Am	8.3	6.5	2.3	—	1.6	—	10.9
^{242m}Am	—	0.6	0.2	—	—	—	0.6
^{243}Am	4.6	3.4	1.2	—	4.1	—	7.2
^{242}Cm	—	—	—	—	—	—	—
^{243}Cm	—	0.3	0.1	—	—	—	0.3
^{244}Cm	0.8	6.4	1.1	—	0.5	—	6.5
^{245}Cm	0.1	2.5	0.5	—	0.1	—	2.5
^{246}Cm	—	—	—	—	—	—	—
^{56}Fe	0.2	—	—	0.4	3.5	—	3.6
^{57}Fe	—	—	—	—	0.4	—	0.4
^{52}Cr	—	—	—	0.1	0.3	—	0.3
^{58}Ni	—	—	—	—	—	—	—
Zr	0.2	—	—	0.2	0.6	—	0.6
^{15}N	—	—	—	1.4	0.3	—	1.4
Pb	0.2	—	—	1.0	8.3	22.4	23.9
Bi	0.3	—	—	1.1	9.7	33.7	35.1
Total[a]	9.6	11.5	3.2	2.0	14.1	40.4	45.5

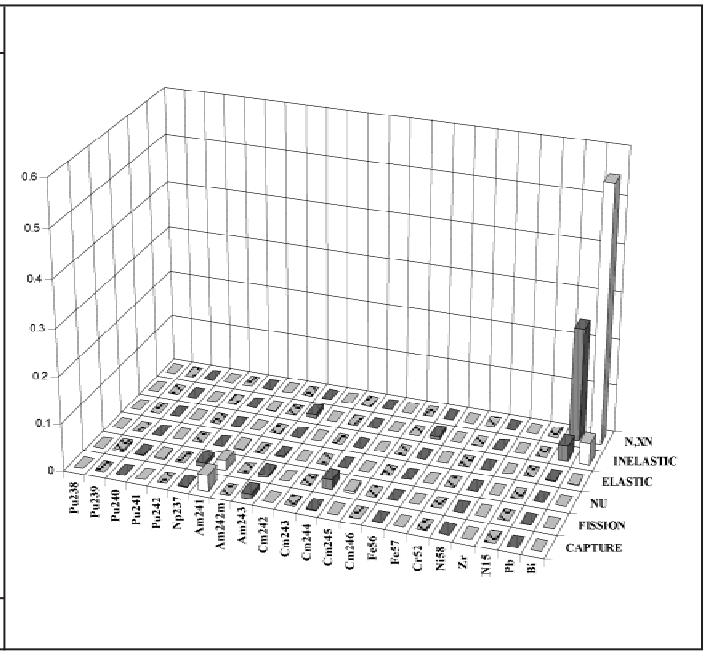

*Uncertainties (%).
[a]Total obtained as the square root of the sum of the squares of individual contributions in row or column.

TABLE XLIII

Total Uncertainty Value*

	Maximum dpa	Maximum He Production	Maximum H Production	Maximum (He Production)/dpa
$\Delta I_{no\_correlation}$[a]	±36.0	±48.0	±34.8	±59.3

*Uncertainty (%).
[a]See text.

As for specific contributions to the uncertainties related to the indirect effects, the Pb and Bi inelastic and $(n,2n)$ cross sections play a major role. The $(n,2n)$ data uncertainty contribution increases from Max dpa to Max H production and has the highest value for Max He production, as expected. Actinide cross-section uncertainties are responsible for spectrum hardening or softening, and their impact is far from negligible. Their impact is the highest for Max dpa and the lowest for Max He production. The results for the Max (He production)/dpa are close to those obtained for Max He production.

VI. THE HYPOTHESIS OF PARTIAL ENERGY CORRELATION

The PEC described in Sec. IV.A, has been applied in the uncertainty analysis for all integral parameters considered. The results are shown in Tables XLIV and XLV.

As a general comment, the total uncertainty values are increased. For example, in the case of k_{eff}, the uncertainty increases from an already significant ±2.77% to ±4.4%. These results, due to the rather arbitrary nature of the correlations introduced, can only be taken to underline the fact that the uncertainties could be higher if realistic energy correlations were introduced. They also indicate the need for more comprehensive covariance data. On the other hand, correlations among cross-section type or among isotopes (e.g., in the case of normalized cross sections) can introduce some anticorrelations, potentially decreasing the overall uncertainty.

VII. AN ASSESSMENT OF CROSS-SECTION TARGET ACCURACY

In the previous sections, we have presented an extensive uncertainty analysis for a large number of

TABLE XLIV

Resulting Uncertainties for the Integral Parameters of the Reference System*

	φ^*	Maximum dpa	Maximum He Production	Maximum H Production	Maximum (He Production)/dpa
$\Delta I_{no\_correlation}$ [a]	±2.74	±29.9	±43.6	±28.5	±45.5
ΔI_{PEC} [a]	±5.07	±48.9	±59.1	±53.1	±67.4

*Uncertainties (%).
[a]See text.

TABLE XLV

Resulting Uncertainties for the Integral Parameters of the Reference System*

	k_{eff}	$\hat{\beta}_{eff}$	$\Delta\rho^{void}$	$\Delta\rho^{cycle}$ (1 yr)	Peak Power
$\Delta I_{no\_correlation}$ [a]	±2.77	±11.3	±35.2	±47.4	±20.5
ΔI_{PEC} [a]	±4.41	±17.4	±59.3	±73.1	±32.4

	Δn^{cycle} [b]						
	^{238}Pu	^{241}Am	^{242m}Am	^{243}Am	^{242}Cm	^{244}Cm	^{245}Cm
$\Delta I_{no\_correlation}$ [a]	±7.33	±15.1	±15.9	±15.3	±12.5	±25.6	±81.2
ΔI_{PEC} [a]	±10.9	±23.8	±23.2	±24.3	±18.3	±37.8	±122.9

*Uncertainties (%).
[a]See text.
[b]1-yr irradiation.

relevant parameters of a system dedicated to transmutation. For most parameters, the results are generally applicable to critical or subcritical versions of such transmuter cores, although somewhat dependent on the choice of the coolant.

In general, the effect of the set of the uncertainties on the cross sections that we have adopted (summarized in Tables IV, V, and VI) is relatively large. These uncertainties can be tolerable in very preliminary design or scenario studies. However, as soon as more precise information is needed, the margins to be taken on the nominal values to provide acceptable conservatism in design or scenario studies, including fuel cycle evaluations, would introduce too many penalties.

If, according to Sec. II.A, one introduces target accuracies in the integral parameters, one can obtain significant quantitative indications of the cross-section accuracies needed.

As for target accuracies in integral parameters, we have defined a tentative first set for the multiplication factor k_{eff}, the external source importance φ^*, the power peak, the Max dpa, the Max He and H production, and the Max (He production)/dpa. The target accuracies are, respectively, ±1, ±2, ±5, ±15, ±15, ±15, and ±15%. These values are, of course, rather arbitrary, but they are consistent with standard requirements for reactor design in early phases of development.

We have used the formulation shown in Sec. II.A with the sensitivity coefficients obtained previously and assuming that the cost parameters λ are set equal to 1. To avoid the introduction of meaningless parameters, we have chosen as unknown d parameters (i.e., as cross sections for which target accuracies are required) only those that globally account for 95% of the overall uncertainty for each integral parameter.

The selected parameters are shown in Table XLVI, together with the initial uncertainty and the new required uncertainty as a result of the minimization procedure outlined in Sec. II.A.

In Table XLVII, we show

1. initial uncertainties on the chosen integral parameters

2. part of the uncertainty accounted for by the selected cross sections

TABLE XLVI

Cross-Section Uncertainties for Selected Cross Sections: Original Uncertainty and Required Uncertainty to Meet Integral Parameter Target Accuracy

Isotope	Cross Section	Group[a]	Original Uncertainty (%)	Required Accuracy (%)	Isotope	Cross Section	Group[a]	Original Uncertainty (%)	Required Accuracy (%)
^{239}Pu	σ_{fiss}	4	6.5	3.4	^{244}Cm	σ_{fiss}	2	40	10.0
		5	4	3.1			3	40	8.5
^{241}Pu	σ_{fiss}	6	10	5.6			4	40	5.0
^{237}Np	σ_{fiss}	3	25	8.0	^{245}Cm	σ_{fiss}	5	30	9.7
		4	25	5.1			6	30	9.6
	ν	4	5	4.1	^{56}Fe	σ_{inel}	4	20	4.9
^{241}Am	σ_{cap}	4	40	7.5	^{15}N	σ_{el}	4	5	3.9
		5	40	5.5	Pb	σ_{inel}	1	40	20.4
		6	40	5.1			2	40	9.8
		7	20	5.9			3	40	10.6
		8	20	6.3			4	40	10.1
		9	20	6.9		$\sigma_{n,2n}$	1	100	21.5
	σ_{fiss}	2	20	5.6	Bi	σ_{inel}	1	40	18.8
		3	20	4.6			2	40	8.1
		4	20	3.9			3	40	9.3
	ν	3	5	3.8			4	40	14.0
		4	5	3.3		$\sigma_{n,2n}$	1	100	17.5
^{243}Am	σ_{cap}	4	40	10.4	σ_{dpa}		1	20	20.0
		5	40	5.5			2	20	12.0
		6	40	5.1			3	20	12.1
		7	20	5.9			4	20	8.8
		8	20	6.3			5	20	20.0
	σ_{fuss}	2	20	7.6			6	20	20.0
		3	20	6.2			7	20	10.9
		4	20	5.4	$\sigma_{(n,\alpha)}$		1	20	10.8
	σ_{inel}	3	50	12.6			2	20	20.0
		4	50	7.6	$\sigma_{(n,p)}$		1	20	15.1
		5	50	12.0			2	20	12.4
		6	50	12.2			3	20	20.0

[a]See energy boundary in Table IV.

TABLE XLVII

Selected Integral Parameters: Uncertainty Due to all Data Uncertainties of Tables IV, V, and VI ($\Delta I_{initial}$); Uncertainty Due to Selected Cross Sections (Tables II and III); Target Accuracies; Resulting Uncertainty from the Minimization Procedure of Sec. II.A

	k_{eff}	φ^*	Power Peak	Maximum dpa	Maximum He Production	Maximum H Production.	Maximum He Production/dpa
$\Delta I_{initial}$	±2.77	±2.74	±20.50	±29.90	±43.60	±28.50	±45.50
$\Delta I_{selected}$	±2.63	±2.63	±19.45	±28.44	±43.43	±27.51	±45.18
$\Delta I_{required}$	±1%	±2%	±5%	±15%	±15%	±15%	±15%
$\Delta I_{resulting}$	±1.1%	±1.0%	±8.2%	±13.0%	±14.8%	±13.7%	±15.3%

3. uncertainties resulting from the new required uncertainties on data (as shown in Table XLVI)
4. imposed target accuracies on the select integral parameters, as given previously.

The results are very encouraging because all the integral parameter uncertainties (except for the power peaking) can be brought within the target accuracy. The case of the power peaking (i.e., resulting uncertainty of approximately ±8% versus the ±5% target value) does not seem to be of major concern.

As for the required cross-section uncertainties, all the values are very reasonable and do not require unrealistic uncertainty reductions. In particular, the required level of uncertainty for the capture, fission, and inelastic cross sections of MAs, is comparable to the level of the uncertainties that have been achieved for major actinides in the past. However, to meet these requirements, a sizeable effort of data reevaluation will be required and probably some new high-accuracy measurements, all below 20 MeV. It is also relevant to notice that the uncertainty required in the case of inelastic and $(n,2n)$ cross sections of Pb and Bi is of the order of ±10 to 20%, according to the energy range, which again looks rather realistic and probably achievable.

The integral parameter selection for assessing target accuracies, accounts for most of the capture and fission cross sections of MAs and inelastic cross sections of both MAs and Pb/Bi. The resulting target accuracies for cross sections will cover most of the potential target accuracy requirements for other integral parameters. To show that, we have used the new uncertainties as indicated in Table XLVII, and we have recalculated the uncertainty of, for example, the void reactivity coefficient. The direct-effects-related uncertainties decrease from ±24.6% (see Sec. IV.D) to ±7.5%, and the indirect-effects-related uncertainty decreases from ±14.2% (see Sec. IV.D) to ±7%. The resulting new total uncertainty on the void coefficient is now approximately ±10 to 15%, well within any target accuracy requirement for this parameter.

VIII. CONCLUSIONS

The sensitivity/uncertainty analysis carried out in this paper allows us to draw some conclusions on the reliability of the present calculation of the systems dedicated to transmutation.

1. The level of uncertainties in integral parameters as assessed is obviously dependent on the assumed values of the cross-section uncertainties and their correlations. However, the present state of knowledge of MA cross sections allows us to state that the uncertainty in the nominal values of the major integral parameters is relevant. Scoping calculations can certainly be performed, but if one takes into account conservative estimates as derived from the uncertainty analysis for performance parameters, some conclusions of conceptual design or scenarios studies can be significantly affected (e.g., beam power needs to drive an ADS, reactivity coefficient assessment and its impact on safety, fuel-cycle-related constraints, like decay heat in a repository, etc.). The reduction of uncertainties would be mandatory in more advanced phases of the studies in order to make sensible choices among options and optimizations.

2. As expected, the most crucial data are fission, capture, and inelastic cross sections of MAs. However, specific data related to decay heat or $\hat{\beta}_{eff}$ assessment are of high relevance. Finally, in the case of a Pb/Bi coolant, the data for these materials should be definitely improved, in particular inelastic and $(n,2n)$ data.

3. High-energy data ($E > 20$ MeV) uncertainties also play a role, but for the transmutation core, only a few data are relevant. Besides (n,α) and (n,p) data for structural materials, only Pb and Bi high-energy data uncertainties are significant. For the major integral parameters considered, there is no serious impact of MA data at $E > 20$ MeV.

High-energy data, of course, play a more relevant role in the assessment of an ADS target performance. In that case, for example, the appropriate assessment of the

activity generated by spallation products will be important, but again the relevant materials will be the potential target material candidates (Pb, Bi, W, etc.).

4. If one defines target accuracies for the integral parameters to allow for more reliable engineering designs, the reduction of the uncertainties, in particular of MA data, which are needed to meet these target accuracies, is significant because one should reach uncertainties of the same order of magnitude of those currently associated with the major actinide data.

5. In this respect, if the nuclear data are reevaluated, one should include not only new differential measurements but, and mostly, integral experiments (like MA sample irradiation in power reactors with variable spectra; see, for example, Ref. 29) because they provide a most powerful tool for global data validation or for data improvement via statistical adjustments. Some of these integral experiments have already been performed in the past but only partially used for nuclear data file updating, and efforts should be devoted to their full exploitation. For very high mass nuclei, some new techniques like accelerator mass spectrometry, applied to tiny quantities of irradiated fuels at relatively high burnup, could provide relevant information with high accuracy.

Finally, future studies related to the impact of nuclear data uncertainties, in particular in the detailed design assessment phase, should rely on variance-covariance data established in a much more rigorous manner, even if adapted (in terms of format and complexity) to user needs.

ACKNOWLEDGMENTS

The authors thank A. d'Angelo for useful suggestions on β_{eff}-related issues. Part of this work was supported by the U.S. Department of Energy, Nuclear Energy Programs, under contract W-31-109-ENG-38

REFERENCES

1. "Actinides and Fission Product Partitioning and Transmutation. Status Assessment Report," OECD Nuclear Energy Agency (1999).

2. M. SALVATORES, I. SLESSAREV, and M. UEMATSU, "A Global Physics Approach to Transmutation of Radioactive Nuclei," *Nucl. Sci. Eng.*, **116**, 1 (1994).

3. T. MUKAYAMA et al., "R and D Strategy for Partitioning and Transmutation under OMEGA Program and Neutron Science Project at JAERI," *Proc. 5th Int. Information Exchange Mtg. Actinides and Fission Product Partitioning and Transmutation*, Mol, Belgium, November 25–27, 1998, EUR 18898 EN, p. 65, OECD/NEA (1999).

4. "A European Roadmap for Developing Accelerator-Driven Systems (ADS) for Nuclear Waste Incineration," Report of the European Technical Working Group on ADS (Apr. 2001).

5. "Accelerator-Driven Systems (ADS) and Fast Reactor (FR) in Advanced Nuclear Fuel Cycles. A Comparative Study," OECD Nuclear Energy Agency (2002).

6. "Comparison Calculations for an Accelerator-Driven Minor Actinides Burner," OECD Nuclear Energy Agency (2002).

7. G. PALMIOTTI, M. SALVATORES, and R. N. HILL, "Sensitivity, Uncertainty Assessment, and Target Accuracies Related to Radiotoxicity Evaluation," *Nucl. Sci. Eng.*, **117**, 239 (1994).

8. G. ALIBERTI, G. PALMIOTTI, M. SALVATORES, and C. G. STENBERG, "Impact of High Energy Data on Uncertainty Assessment of ADS Neutronic Design," *Trans. Am. Nucl. Soc.*, **87**, 525 (2002).

9. G. PALMIOTTI, P. J. FINCK, I. GOMES, B. MICKLICH, and M. SALVATORES, "Uncertainty Assessment for Accelerator-Driven-System," presented at Int. Conf. Global '99: Future Nuclear Systems, Jackson, Wyoming, August 29–September 3, 1999.

10. *Uncertainty Analysis*, Y. RONEN, Ed., CRC Press, Boca Raton, Florida (1988); see also J. H. MARABLE et al., *Advances in Nuclear Science and Technology*, Vol. 14, J. LEWINS and A. BECKER, Eds., Plenum Press, New York (1982).

11. A. GANDINI, *Uncertainty Analysis*, Y. RONEN, Ed., CRC Press, Boca Raton, Florida (1988); see also E. GREENSPAN, *Advances in Nuclear Science and Technology*, Vol. 14, J. LEWINS and A. BECKER, Eds., Plenum Press, New York (1982).

12. L. N. USACHEV and Y. BOBKOV, "Planning an Optimum Set of Microscopic Experiments and Evaluations to Obtain a Given Accuracy in Reactor Parameter Calculations," INDC CCP-19U, International Atomic Energy Agency (1972).

13. A. GANDINI, G. PALMIOTTI, and M. SALVATORES, "Equivalent Generalized Perturbation Theory (EGPT)," *Ann. Nucl. Energy*, **13**, *3*, 109 (1986).

14. J. M. KALLFELZ, G. B. BRUNA, G. PALMIOTTI, and M. SALVATORES, "Burnup Calculations with Time-Dependent Generalized Perturbation Theory," *Nucl. Sci. Eng.*, **62**, 304 (1977).

15. M. L. WILLIAMS, "Development of Depletion Perturbation Theory for Coupled Neutron/Nuclide Fields," *Nucl. Sci. Eng.*, **70**, 20 (1979).

16. J. R. WHITE, "The DEPTH-CHARGE Static and Time-Dependent Perturbation/Sensitivity System for Nuclear Reactor Core Analysis," ORNL/CSD-78, Oak Ridge National Laboratory (1981).

17. G. PALMIOTTI, R. F. BURSTALL, E. KIEFHABER, W. GEBHARDT, and J. M. RIEUNIER, "New Methods Developments and Rationalization of Tools for LMFBR Design in the Frame of the European Collaboration," presented at FR'91 Int. Conf. Fast Reactors and Related Fuel Cycles, Kyoto, Japan, October 28–November 1, 1991.

18. G. PALMIOTTI, J. M. RIEUNIER, C. GHO, and M. SALVATORES, "Optimized Two-Dimensional S_n Transport (BISTRO)," *Nucl. Sci. Eng.*, **104**, 26 (1990).

19. M. J. BELL, "The ORNL Isotope Generation and Depletion Code," Oak Ridge National Laboratory (May 1973).

20. "The JEF-2.2 Nuclear Data Library," Report 17, OECD/NEA (Apr. 2000).

21. M. B. CHADWICK, P. G. YOUNG, S. CHIBA, S. C. FRANKLE, G. M. HALE, H. G. HUGHES, A. J. KONING, R. C. LITTLE, R. E. MacFARLANE, R. E. PRAEL, and L. S. WATERS, "Cross-Section Evaluations to 150 MeV for Accelerator-Driven Systems and Implementation in MCNPX," *Nucl. Sci. Eng.*, **131**, 293 (1999).

22. E. FORT, Private Communication (2001).

23. "Present Status of Minor Actinide Data," NEA/WPEC-8, OECD/NEA (1999).

24. A. D'ANGELO, "A Total Delayed Neutron Yields Adjustment Using Integral Measurements," *Proc. Int. Conf. PHYSOR'90*, Marseille, France, April 23–27, 1990.

25. R. W. MILLS, "Fission Product Yield Evaluation," PhD Thesis, University of Birmingham, United Kingdom (1995).

26. G. P. GROUILLER, Private Communication (1990).

27. J. REBAH, PhD Thesis, University of Paris (1998).

28. D. G. NABEREJNEV and M. SALVATORES, "Irradiation of Structural Materials in Spallation Neutron Sources," *Trans. Am. Nucl. Soc.*, **86**, 425 (2002).

29. M. SALVATORES, "Future Nuclear Power Systems and Nuclear Data Needs," presented at Int. Conf. on Nuclear Data for Science and Technology, Tsukuba, Japan, October 7–12, 2001.